Numerical Heat Transfer, Part B: Fundamentals

https://www.tandfonline.com/toc/unhb20/current

Accepted February 6th, 2024.

NUMERICAL STUDY OF LINEAR AND NONLINEAR STABILITY IN DOUBLE-DIFFUSIVE HADLEY-PRATS FLOW THROUGH A HORIZONTAL POROUS LAYER WITH SORET AND INTERNAL HEAT SOURCE EFFECTS

M. Rafeek [1], G. J. Reddy[1,*], Anjanna Matta[2], Hussain Basha[3,*] and O. Anwar Bég[4]

[1]Laboratory on Computational Fluid Dynamics, Department of Mathematics, Central University of Karnataka, Kalaburagi, India.

[2]Department of Mathematics, Faculty of Science & Technology, The ICFAI Foundation for Higher Education, Hyderabad, India.

[3]Department of Mathematics, Government Degree College, Sindhanur-584128, Karnataka, India.

[4]Professor, Multi-physical Engineering Sciences, Aeronautical/ Mechanical Engineering Department, School of Science, Engineering and Environment, Salford University, Manchester M54WT, UK.

[*]Corresponding Authors Emails: gjr@cuk.ac.in; hussainbmaths@gmail.com

Abstract

Numerical analysis is constructed to study the onset of double-diffusion convection mechanism through an infinite parallel permeable channel with heat generation, mass flow and Soret impacts. Homogenous isotropic Darcy's flow model is deployed to elucidate the porous features. The roll instabilities pertaining to longitudinal and transverse cases are examined through linear and nonlinear stability analysis. The unit-less eigenvalue problem is constructed through linear and nonlinear stability assumptions and which is solved numerically using a fourth order Runge-Kutta scheme. The critical values of wave and thermal Rayleigh parameters are evaluated. Extended graphical and tabular visualization is presented to describe the onset of convection mechanism. The results of this semi-numerical investigation may be useful in environmental, geothermal and chemical engineering processes. In addition, the critical R_z value is also determined for a range of thermo-physical numbers. Significant modifications in the flow patterns are computed with mass flow parameter and vertical thermal and solutal Rayleigh number. With an increment in Soret (thermo-diffusive) parameter Sr the regime become more unstable. Based on the nonlinear stability analysis, an elevation in solutal Rayleigh number also induces earlier instability. The collective influence of Lewis number and horizontal concentration parameter is observed to render the system more stable.

Keywords: Double-diffusive thermo-convective instability; eigenvalues; critical wave number; Porous medium; Soret thermo-diffusion; nonlinear; solutal Rayleigh number; Energy method; Lewis number; numerical solutions.

1. Introduction

The physical situation of double diffusion thermo-solutal-convection instabilities in a saturated flat infinite absorbent layer featuring internal heat generation and thermo-diffusive Soret effects is fundamental to a wide range of environmental and industrial systems including geothermal reservoirs [1], underground energy transport [2], groundwater transport [3], chemical engineering micro/nano-devices [4], oil recovery [5], food processing, nuclear reactors cooling, waste disposal of nuclear reactors, soil remediation. Also, in practical applications [6-7], the fluid layer was steadily and uniformly illuminated with light emitted by a sodium vapor lamp and this radiation acted as an internal heat source. This type of convection mechanism is penetrative, which is modeled via an internal heat source. If this internal heat source is applied to the porous medium region then it gives the system which is equivalent in model such as salt gradient layer in solar pond. Usually, this type of convection process arises in sea water flow and mantle flow in the earth's crust. Further, porous media further arise in many areas of biomedical engineering including tissue, bone etc. Theoretical studies of viscous flows in such media provide an important compliment to experimental investigations. Porous media are inherently complex and generally heterogeneous. They may also feature tortuosity, anisotropic permeability and other geometrical features. To simulate transport in such media, a variety of methodologies are available including drag force models, multi-scale models, hierarchical models, spatially periodic models and so on. The most popular approach however remains the Darcy model which assumes that flow rate is linearly proportional to the pressure drop. It is generally limited to viscous-dominated flows and Reynolds numbers of about 10, after which inertial effects are invoked. Investigations of the beginning of thermo-solute convection through absorbent media have often deployed the Darcian model. This has provided a good framework for evaluating many complex characteristics associated with hydrodynamic, thermal and solutal instability including stability analysis and etc.

Hadley-Prats flow (which originated in meteorology for the distribution of winds in the atmosphere) and describes the transport in a shallow fluid-saturated porous layer generated via an inclined temperature gradient, specifically the thermo-convective circulation induced in the central section of the layer. It has received significant interest in the fluid dynamics community. The fluid motion produced at the central regime of the flow due to the thermal differences is essentially a 1-dimensional flow and can be expressed for Newtonian fluids in terms of the Navier-Stokes equations. Horton and Rogers [8] and Lapwood [9] described the thermal transport mechanism in an infinite parallel regime caused by the temperature gradients at the central portion. They established a robust platform for subsequent studies. Further, the thermal convection process through the parallel channel region with thermal production/absorption was later addressed owing geothermal energy and other applications by many investigators. Extended linear hydrodynamic stability discussion was depicted by Nield [10]. Nield's analysis was further generalized to incorporate the influence of viscous dissipation on transport characteristics. Barletta et al. [11] considered the flat inclined parallel Darcian porous channel with inside heat production/sink and equivalent isothermal boundaries using a linear instability analysis. They studied the case where the upper boundary is isothermal and the lower one is isothermal/adiabatic and identified that the longitudinal rolls (i. e. normal modes with wave vector normal to the basic flow) exhibit the highest instability. They further observed that provided the inclination angle is lower than a critical (threshold) value, neutrally stable transverse modes can grow with elapse in time. Nield and Bejan [12] described the temperature instability through permeable channel was significantly discussed in view of practical applications. Hill [13] investigated the temperature and concentration instability in horizontal permeable channel for the case in which inside heat production varies with respect to solute concentration. Weber [14] presented the first comprehensive analysis of mono-diffusive non-homogeneous temperature gradients and it applicable to small temperature gradients. Dual thermal/solutal diffusive stability flows in permeable media were explored by Ingham and Pop [15] and Vafai [16] and many other investigations have been reviewed in Nield and Bejan [12].

Nield et al. [17] analyzed the dual diffusion convection Hadley-Prats motion under inclined solutal and thermal slopes in an infinite horizontal porous layer. Mass flow through a flat permeable channel was analyzed theoretically by Manole et al. [18]. Barletta and Nield [19] computed the Hadley-Prats fluid motion through a flat permeable channel under inclined thermal difference with viscous heating contribution. They parameterized the problem to show that it is dictated by four dimensionless numbers. They computed both critical wave and

Rayleigh parameters and determined that longitudinal rolls are the dominant mode of mode of instability compared with transverse disturbances. In all these studies generally linear stability analysis was used to characterize the critical parameters affecting the sensitivity of the thermal convection in Darcy porous media. However more recently nonlinear stability computations have also been reported in the literature. Matta et al. [20] used shooting quadrature to compute eigenvalue solutions for both linear and nonlinear stability in Hadley-Prats motion with mass diffusion and internal thermal generation in an infinite horizontal porous layer under dual diffusive conditions. They considered the concentration dependent inside thermal source and computed the critical thermal Rayleigh number. Their solutions showed that for the linear case, elevation in Rayleigh parameter serves to stabilize the regime for Rayleigh number but in non-linear study, significant instability is induced with large concentration flow rates and heat source intensity. Matta et al. [21] extended this work to consider the additional impact of gravitational variation.

Many mathematical investigations such as [22, 23] discussed the thermal convection mechanism under heat production case due to their enhanced applications in geophysical fluid motions in which mantle of earth's is heated from inside and also in materials processing where hot spots are deployed for manipulation of material characteristics. Internal heat generation refers to the production of heat within a fluid system due to chemical reactions or other physical process. It has applications in industrial process such as chemical manufacturing and material processing. Moreover, it has applications in electronic devices and geothermal systems such as mantle convection and generation of geothermal energy. Schwiderskei and Schwabh [24] and Trittond and Zarraua [25] provided important experimental results for a range of systems including electrically heated shallow layers and purely thermally heated regimes, identifying a diverse array of convection patterns including classical rolls, hexagons with upward flow at the cores and also hexagons with downward flow at their cores. Their investigations also showed that internal heat generation effects under free convection conditions are heavily reliant on vertical motion and complex circulations in the regime. Parthiban and Patil [26] conducted thermal instability analysis with uncertain heated boundaries under the effect of inside thermal source and inclined thermal gradients. Parthiban and Patil [27] extended their study by considering an anisotropic porous layer with uniformly distributed internal heat generation. They employed the Galerkin scheme to compute the impact of thermal differences in a horizontal layer owing to the differential warming of boundary wall on the beginning of convective flow, identifying that initially the convective circulation is assisted with interior thermal generator with effective thermal differences. They further observed that, enlarged temperature difference amplifies the acute Rayleigh parameter. Guo and Kaloni [28] applied the energy method by implementing the coupling parameters to understand onset of convection motivated by inclined thermal and solutal gradients in a horizontal porous layer. Similarly, Kaloni and Qiao [29-31] extensively studied the Hadley-Prats nonlinear convection flow problems with different physical effects by using energy method. Also, Kaloni and Lou [32] studied the energy method to investigate nonlinear stability analysis for the viscoelastic fluid. Recently, Matta et al. [33] investigated the thermo-convective stability with mass flux and internal heat source effects. The effects of concentration based internal heat generation and gravity variation were further investigated by Matta [34].

In thermo-solutal (double diffusive) convection in which heat and mass transfer occur simultaneously, the interdependency between the energy and solutal (concentration) fluxes can exert a dramatic influence on flow characteristics. The fluxes associated with both temperature and concentration fields feature in additional body force terms in the momentum equations. Mass flux may be induced also by both inclined thermal gradients and solutal gradients. The horizontal concentration flux produced due to the temperature differences is known as the Soret effect. The Soret effect, also known as thermophoresis is a phenomenon in which particles or solutes in a fluid move in response to a temperature gradient. The key factor is the variation of mass diffusion with temperature gradient. The Soret effect is often observed in mixtures of different components such as in colloidal suspensions, gases and liquids. Researchers and scientists study the Soret effect to better understand mass transport phenomena and to develop applications such as separation techniques and controlled drug delivery systems. The diffusive-thermal effect or Dufour effect is related to the temperature flux caused by concentration gradients. While both effects are based on the classical Fickian species diffusion and Fourier heat conduction models, the Dufour impact may be ignored in fluids due to its small order when compared to Soret effect, as confirmed by Platten and Legros [35] and Larre et al. [36]. The thermal and solutal convection in a horizontal porous layer with the Soret effect has, in particular, attracted the attention of several authors. Hurle and Jakeman [37] discussed the different processes for oscillatory convection modes under Soret effect. Bahloul [38] studied analytically and numerically the Soret-induced convection in a horizontal porous layer. Narayana et al. [39] presented a detailed stability analysis of the Soret-driven thermosolutal convection of Hadley flow in a horizontal porous layer. Roy and Murthy [40] examined the collective effects of Soret thermo-diffusion and viscous dissipation on double-diffusive convective instability effect. They noted that for the enlarging Soret number, the transverse rolls exhibit the greatest instability even at comparatively low values of viscous heating parameter. They further showed that at higher values of viscous heating, the transverse rolls become more unstable although only for non-positive values of the Soret parameter. Further investigations include Deepika [41] who conducted a rigorous linear and nonlinear stability study of Soret impact on convection double diffusion transport mechanism through saturated porous layer. Linear and nonlinear stability analysis of thermohaline convection of a Casson fluid in a porous layer was implemented by Shiva et al. [42]. Reshmi and Murthy [43] studied about the onset of convective instability analysis of horizontal throughflow in a porous layer with inclined thermal and solutal gradients. They have employed a more general Brinkman model, and disused the accountability of all the factors like viscous dissipation, throughflow, inclined gradients, etc. for both transverse and longitudinal rolls which are the most and least stable modes through linear stability analysis. Recently, Rafeek et al. [44] implemented the mono-diffusive Hadley flow with internal heat source and viscous dissipation effect by considering lower infinite plate have more temperature as compared with upper infinite plate and it causes the buoyancy force due to the variation in density which leads to convection. Here, the authors are discussed only the linear instability analysis and solved the Eigenvalue problem encountered from the linear instability analysis by using RK-4 shooting numerical technique.

A scrutiny of the literature has revealed that thus far a computational linear and nonlinear stability investigation of the collective impacts of inside thermal source, mass flow and Soret thermo-diffusion on the beginning of double-diffusive Hadley-Prats convective transport through a shallow Darcian porous medium has not been reported. This is the focus and novelty of the current work which has immediate applications in geophysical transport modelling and industrial manufacturing in addition to atmospheric fluid dynamics [45]. The mathematical model developed utilizes the Darcy law for the homogenous isotropic porous material. Linear and nonlinear stability investigation is performed for both cases. The developed non-dimensional eigenvalue problems derived from linear and nonlinear stability analyses are solved numerically using a fourth order Runge-Kutta scheme. Extensive interpretation of the numerical concerning to onset convection is also included. Substantial visualization of the solutions is included for the effects of a range of parameters such as the vertical thermal and solutal Rayleigh number, Soret (thermo-diffusive) parameter, Lewis number and horizontal concentration parameter.

2. Mathematical formulation of the physical problem

The physical regime consists of a homogeneous infinite horizontal Darcian porous layer saturated with a Newtonian fluid. The boundaries are iso-solutal and the isothermal stationary plates located a distance d apart (height of the shallow channel). The upward vertical axis is orientated in the z'-direction and the plates are in the horizontal $(x' - y'\ plane)$. The imposed horizontal temperature and solutal gradients vectors are $\left(\beta_{\theta_x}, \beta_{\theta_y}\right)$ and $\left(\beta_{C_x}, \beta_{C_y}\right)$ with internal heat generation Q' and net mass flow along the x'-direction with velocity u_0 also in the x'-direction. Figure 1 depicts the investigated geometry.

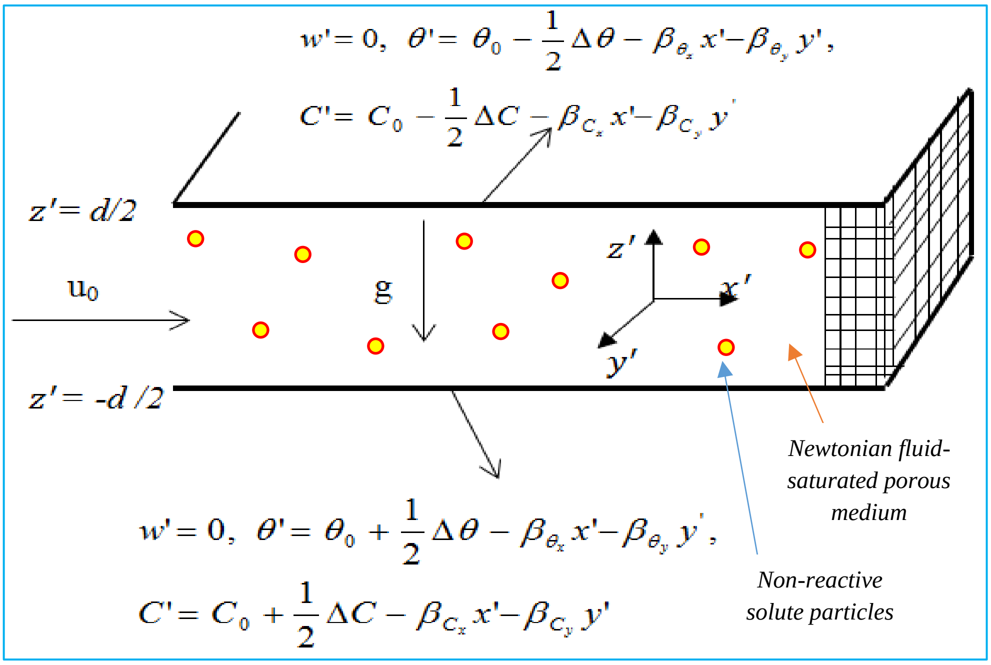

Figure 1: The physical system of investigated problem.

A homogeneous concentration variation ΔC and temperature variation $\Delta\theta$ is considered at the horizontal boundaries. Temperature and concentration of the fluid varies from position to position as the percolating fluid moves along the horizontal porous medium intercalated between the infinite parallel plates. Oberbeck-Boussinesq predictions are applied (density variations are assumed to be adequately insignificant to neglect except in the buoyancy terms). Darcy's rule is deployed for the porous material. Density ρ_f' of the fluid is defined with the familiar equation $\rho_f' = \rho_o[1 - (\theta' - \theta_o)\gamma_\theta - (C' - C_o)\gamma_C]$. Here θ' is the temperature, C' is the solute concentration, γ_C and γ_θ are coefficients of species and temperature, ρ_0 is density when concentration is C_0 and temperature difference is θ_0. Under these approximations, the vector form of the conservation equations for mass, momentum, energy and species diffusion (concentration) for the thermal solutal convection in the horizontal porous layer are defined as follows:

$$\nabla'.q' = 0, \tag{1}$$

$$\frac{\mu}{K}q' + \nabla' P' - \rho_f' g\boldsymbol{k} = 0, \tag{2}$$

$$\emptyset\left(\frac{\partial C'}{\partial t'}\right) + q'.\nabla' C' = D_m \nabla'^2 C' + D_s \nabla'^2 \theta', \tag{3}$$

$$(\rho c)_m \frac{\partial \theta'}{\partial t'} + (\rho c_P)_f q'.\nabla'\theta' = k_m \nabla'^2 \theta' + Q'. \tag{4}$$

Here Eq. (1) corresponds to mass conservation in incompressible flow. The necessary constraints are listed below:

$$\left.\begin{array}{l} z' = -\frac{1}{2}d: w' = 0, C' = C_0 + \frac{\Delta C}{2} - \beta_{C_x}x' - \beta_{C_y}y', \theta' = \theta_0 + \frac{\Delta\theta}{2} - \beta_{\theta_x}x' - \beta_{\theta_y}y' \\ z' = \frac{1}{2}d: w' = 0, C' = C_0 - \frac{\Delta C}{2} - \beta_{C_x}x' - \beta_{C_y}y', \theta' = \theta_0 - \frac{\Delta\theta}{2} - \beta_{\theta_x}x' - \beta_{\theta_y}y' \end{array}\right\} \tag{5}$$

Pertaining to Eqs. (1)-(5), the velocity vector is $q' = (u', v', w')$, P' denotes the pressure. Here, μ, c, D_s k_m, $D_{m,}$ $g, K, \boldsymbol{k}$, $\vartheta, \emptyset$, c_p and ρ_0 explores the viscosity, specific heat, Soret parameter, thermal conductivity, solutal diffusivity, gravitation field, permeability of permeable medium, vector along z'-path, kinematic viscosity, porosity of the medium, specific heat of fluid and density of liquid. Below listed unite-less quantities are used in this investigation.

$$\left.\begin{array}{l} (x, y, z) = \frac{1}{d}(x', y', z'), Q = \frac{d^2 Q'}{k_m \Delta\theta}, t = \frac{\alpha_m t'}{a d^2}, (u, v, w) = q = \frac{d q'}{\alpha_m}, P = \frac{K(P' + \rho_0 g z')}{\mu \alpha_m} \\ \theta = \frac{R_z(\theta' - \theta_0)}{\Delta\theta}, \quad C = \frac{C_z(C' - C_0)}{\Delta C}, \quad \alpha_m = \frac{k_m}{(\rho c_p)_f}, \quad a = \frac{(\rho c)_m}{(\rho c_p)_f} \end{array}\right\} \tag{6}$$

Here a is describes the relation between porous media thermal capacity and fluid medium, α_m denote the temperature diffusivity, Q be the inside thermal production number. Using these non-dimensional formulae, the considered Eqs. (1)-(5) are reduced as follows:

$$\nabla.q = 0, \tag{7}$$

$$q + \nabla P - \left(\frac{1}{Le}C + \theta\right)\boldsymbol{k} = 0, \tag{8}$$

$$\left(\frac{\emptyset}{a}\right)\frac{\partial C}{\partial t} + q.\nabla C = \frac{1}{Le}\nabla^2 C + Sr\nabla^2\theta, \tag{9}$$

$$\frac{\partial\theta}{\partial t} + q.\nabla\theta = \nabla^2\theta + QR_z. \tag{10}$$

Also, the defined constraints for the considered problem are listed below:

$$
\left.\begin{aligned}
z = -\tfrac{1}{2}: \quad w = 0, \quad C = \tfrac{C_z}{2} - C_x x - C_y y, \quad \theta = \tfrac{R_z}{2} - R_x x - R_y y, \\
z = \tfrac{1}{2}: \quad w = 0, \quad C = -\tfrac{C_z}{2} - C_x x - C_y y, \quad \theta = -\tfrac{R_z}{2} - R_x x - R_y y
\end{aligned}\right\} \tag{11}
$$

Here, in Eqs. (7)-(11), the perpendicular, flat temperature and solute Rayleigh parameters are depicted as R_z,C_z, R_x ,R_y , C_x and C_y respectively, Sr represents the Soret number and Le represents the Lewis number (ratio of thermal and species diffusivities) and M is net dimensionless Peclet number. These parameters are defined as follows:

$$
R_z = \frac{\rho_0 g \gamma_\theta K d \Delta\theta}{\mu \alpha_m}, C_z = \frac{\rho_0 g \gamma_C K d \Delta C}{\mu D_m}, R_x = \frac{\rho_0 g \gamma_\theta K d^2 \beta_{\theta_x}}{\mu \alpha_m}, C_x = \frac{\rho_0 g \gamma_C K d^2 \beta_{C_x}}{\mu D_m},
$$

$$
R_y = \frac{\rho_0 g \gamma_\theta K d^2 \beta_{\theta_y}}{\mu \alpha_m}, C_y = \frac{\rho_0 g \gamma_C K d^2 \beta_{C_y}}{\mu D_m}, Sr = \frac{D_s \gamma_C}{D_m \gamma_\theta}, \quad Le = \frac{\alpha_m}{D_m}, \; M = \frac{u_0 d}{\alpha_m}. \tag{12}
$$

From the above boundary conditions Eq. (11), it is interesting to note that, vertical and thermal and solute Rayleigh parameters all arise. The conditions on the temperatures and concentration at the boundaries permit the linear variations in thermal and concentration fields to be simulated.

3. Time-independent outcomes

The Eqs. (7)-(10) admit elementary time-independent results under the defined constraints at the flat boundaries, as below:

$$
\theta_s = \widetilde{\theta}\,(z) - R_x x \; - R_y y, \qquad C_s = \widetilde{C}\,(z) - C_x x - C_y y, \tag{13}
$$

$$
(u_s\,, v_s\,, w_s\;) = (u(z),\; v(z)\,,\; 0), \qquad P_s = P(x,y,z). \tag{14}
$$

The steady state solutions emerging are:

$$
u_s = -\frac{\partial P}{\partial x}, \qquad v_s = -\frac{\partial P}{\partial y}, \tag{15}
$$

$$
0 = -\frac{\partial P}{\partial z} + \left[\frac{1}{Le}\left(\tilde{C}(z) - C_x x - C_y y\right) + \left(\tilde{\theta}(z) - R_x x \; - R_y y\;\right)\right], \tag{16}
$$

$$
D^2\tilde{\theta}(z) = \; -u_s R_x - v_s R_y - Q R_z\,, \tag{17}
$$

$$
D^2\tilde{C}(z) = Le\left[-C_x u_s - C_y v_s + Sr(\lambda_1 z + M R_x + Q R_z)\right]. \tag{18}
$$

Where:

$$
\lambda_1 = R_x^2 + R_y^2 + \left(\frac{R_x C_x + R_y C_y}{Le}\right). \tag{20}
$$

Here, $D = \frac{d}{dz}$, the net mass flow in the x-direction is $\int_{-\frac{1}{2}}^{\frac{1}{2}} u(z)\, dz = M$ and in y – direction is $\int_{-\frac{1}{2}}^{\frac{1}{2}} v(z)\, dz = 0$ where M is Peclet number and quantifies the strength of the mass flow. Basic steady state solutions now emerge for the velocity components, temperature and the solute concentration in the porous medium, as follows:

$$u_s = \left(R_x + \frac{C_x}{Le}\right) z + M\,, \qquad v_s = \left(R_y + \frac{C_y}{Le}\right) z, \qquad w_s = 0, \tag{21}$$

$$\tilde{C} = -C_z z + A\,, \qquad \tilde{\theta} = -R_z z + B. \tag{22}$$

Here the unknowns A and B take the following definitions:

$$A = \frac{\lambda_2}{24}(z - 4z^3) + \frac{\lambda_3}{2}\left(z^2 - \frac{1}{4}\right), \tag{23}$$

$$B = \frac{\lambda_1}{24}(z - 4z^3) - (MR_x + QR_z)\left(\frac{z^2}{2} - \frac{1}{8}\right), \tag{24}$$

The parameters λ_2 and λ_3 are defined as:

$$\lambda_2 = C_x^2 + C_y^2 + Le\left(C_x R_x + C_y R_y + Sr\left(R_x^2 + R_y^2\right)\right) + Sr\left(R_x S_x + R_y S_y\right),$$

$$\lambda_3 = Le\, Sr\,(MR_x + QR_z). \tag{25}$$

The steady state velocity solutions given by Eq. (21) correspond to classical *Hadley-Prats* flow.

4. Disturbance equations

This section comprises the perturbation of fundamental steady state solutions as $q = q_s + \bar{q}$, $\theta = \theta_s + \bar{\theta}$, $C = C_s + \bar{C}$, and $P = P_s + \bar{P}$. Letting these disturbances in the non-dimensional Eqs. (7)-(10) and results below listed perturbed expressions:

$$\nabla.\bar{q} = 0, \tag{26}$$

$$\bar{q} + \nabla\bar{P} - \left(\frac{1}{Le}\bar{C} + \bar{\theta}\right)\boldsymbol{k} = 0, \tag{27}$$

$$\left(\frac{\phi}{a}\right)\frac{\partial\bar{C}}{\partial t} + q_s.\nabla\bar{C} + \bar{q}.\nabla C_s + \bar{q}.\nabla\bar{C} = \frac{1}{Le}\nabla^2\bar{C} + Sr\nabla^2\bar{\theta}, \tag{28}$$

$$\frac{\partial\bar{\theta}}{\partial t} + q_s.\nabla\bar{\theta} + \bar{q}.\nabla\theta_s + \bar{q}.\nabla\bar{\theta} = \nabla^2\bar{\theta}. \tag{29}$$

In the above Eqs. (26)-(29) the following definitions apply:

$$\nabla C_s = -\left(C_x, C_y\,, C_z - \tilde{A}\right), \qquad \nabla\theta_s = -\left(R_x, R_y, R_z - \tilde{B}\right),$$

$$\tilde{A} = \frac{\lambda_2}{24}(1 - 12z^2) + \lambda_3 z,$$

$$\tilde{B} = \frac{\lambda_1}{24}(1-12z^2) - (MR_x + QR_z)z. \tag{30}$$

In addition, the constraints at the flat boundaries are stated below:

$$\bar{w} = 0, \qquad \bar{C} = 0\,, \qquad \bar{\theta} = 0\,, \quad \text{at} \quad z = \mp\frac{1}{2}. \tag{31}$$

Here, Eq. (31) shows the absence of porous material and orthogonal fluid motion with thermal and mass diffusion disturbances rising at the borders.

5. Linear stability analysis

Here, the temperature and solute linear stability is examined. For implementing linear instability study, the non-linear factors and products of disturbances appearing in Eqs. (26)-(29) are ignored. Thus, the resultant, linear disturbance expressions are:

$$\nabla.\bar{q} = 0, \tag{32}$$

$$\bar{q} + \nabla\bar{P} - \left(\frac{1}{Le}\bar{C} + \bar{\theta}\right)\boldsymbol{k} = 0, \tag{33}$$

$$\left(\frac{\phi}{a}\right)\frac{\partial\bar{C}}{\partial t} + q_s.\nabla\bar{C} + \bar{q}.\nabla C_s = \frac{1}{Le}\nabla^2\bar{C} + Sr\nabla^2\bar{\theta}, \tag{34}$$

$$\frac{\partial\bar{\theta}}{\partial t} + q_s.\nabla\bar{\theta} + \bar{q}.\nabla\theta_s = \nabla^2\bar{\theta}\,. \tag{35}$$

Linear constraints at the walls of geometry become:

$$\bar{w} = 0, \qquad \bar{C} = 0\,, \qquad \bar{\theta} = 0 \quad \text{at} \quad z = \mp\frac{1}{2}. \tag{36}$$

The linearized perturbation equations reduce to the following:

$$\nabla.\bar{q} = 0, \tag{37}$$

$$\bar{q} + \nabla\bar{P} - \left(\frac{1}{Le}\bar{C} + \bar{\theta}\right)\boldsymbol{k} = 0, \tag{38}$$

$$\left(\frac{\phi}{a}\right)\frac{\partial\bar{C}}{\partial t} + u_s\frac{\partial\bar{C}}{\partial x} + v_s\frac{\partial\bar{C}}{\partial y} - C_x\bar{u} - C_y\bar{v} + \bar{w}\left(D\tilde{C}\right) = \frac{1}{Le}\nabla^2\bar{C} + Sr\nabla^2\bar{\theta}, \tag{39}$$

$$\frac{\partial\bar{\theta}}{\partial t} + u_s\frac{\partial\bar{\theta}}{\partial x} + v_s\frac{\partial\bar{\theta}}{\partial y} - R_x\bar{u} - R_y\bar{v} + \bar{w}\left(D\tilde{\theta}\right) = \nabla^2\bar{\theta}. \tag{40}$$

In the above Eqs. (37)-(40), the values of $D\tilde{C}$ and $D\tilde{\theta}$ are as follows:

$$D\tilde{C} = -C_z + \frac{\lambda_2}{24}(1-12z^2) + \lambda_3 z\,,$$

$$D\tilde{\theta} = -R_z + \frac{\lambda_1}{24}(1-12z^2) - (MR_x + QR_z)z. \tag{41}$$

Meanwhile the resulting system of differential equations are linear and autonomous. Therefore, adopting a Fourier mode solution to Eqs. (38)-(40) along with the boundary conditions in Eq. (36) yields solutions of the format:

$$[\bar{q}, \bar{\theta}, \ \bar{C}, \ \bar{P}\ ] = [q(z), \theta(z), C(z)\ , P(z)]\ exp\{i(kx + ly - \sigma t)\} \tag{42}$$

Eliminating the pressure term P from the Eq. (38) we obtain:

$$(D^2 - \alpha^2)w + \left(\frac{C}{Le} + \theta\right)\alpha^2 = 0, \tag{43}$$

$$\left(\frac{1}{Le}(D^2 - \alpha^2) + i\left(\frac{\phi}{a}\right)\sigma - iku_s - ilv_s\right)C + \frac{i}{\alpha^2}\left(kC_x + lC_y\right)Dw - \left(D\tilde{C}\right)w + Sr(D^2 - \alpha^2) = 0, \tag{44}$$

$$(D^2 - \alpha^2 + i\sigma - iku_s - ilv_s)\theta + \frac{i}{\alpha^2}\left(kR_x + lR_y\right)Dw - \left(D\tilde{\theta}\right) = 0. \tag{45}$$

The above Eqs. (43) – (45) have conditions $w = \theta = C = 0$ satisfied at both the boundaries $z = \frac{1}{2}$ and $z = \frac{-1}{2}$. Here the following definitions are used:

$$D\tilde{C} = -C_z + \frac{\lambda_2}{24}(1 - 12z^2) + \lambda_3 z\ ,\ \ D\tilde{\theta} = -R_z + \frac{\lambda_1}{24}(1 - 12z^2) - (MR_x + QR_z)z. \tag{46}$$

The eigenvalue problem is therefore defined in terms of the critical parameter being the vertical thermal Rayleigh number R_z with $\sigma, R_x, R_y,\ Q, Sr, k, \alpha, \phi, Le, C_x, C_y, C_z$ and l as variables. Furthermore $\alpha = \sqrt{k^2 + l^2}$ represents the global wave number and $i = \sqrt{-1}$.

6. Nonlinear stability analysis

In this section, the non-linear stability analysis is conducted based on energy functionals. To determine global non-linear instability limits, authors multiply Eqs. (27)-(29) by $\bar{q}, \bar{\beta}$ and $\bar{\theta}$ and integrate about the typical periodicity cell, indicated with Ω and which gives the following identities:

$$\|\bar{q}\|^2 = \langle\bar{\theta}\,\bar{w}\rangle + \langle\bar{\beta}\,\bar{w}\rangle, \tag{47}$$

$$\frac{Le\,\phi}{2a}\frac{d\|\bar{\beta}\|^2}{dt} = -\langle(\bar{q}.\nabla C_s)\bar{\beta}\rangle - \left\|\nabla\bar{\beta}\right\|^2 - Sr\langle\nabla\bar{\theta}.\nabla\bar{\beta}\rangle, \tag{48}$$

$$\frac{1}{2}\frac{d\|\bar{\theta}\|^2}{dt} = -\langle(\bar{q}.\nabla\theta_s)\bar{\theta}\rangle - \left\|\nabla\bar{\theta}\right\|^2. \tag{49}$$

Here $\bar{\beta} = \frac{\bar{C}}{Le}$, and $\langle\cdot\rangle$ denotes the integration over Ω and $\|\cdot\|$ represents the $L^2(\Omega)$ norm. The following energy functional is next defined following Straughan [46]:

$$E(t) = \frac{\xi}{2}\left\|\bar{\theta}\right\|^2 + \frac{\eta Le\phi}{2a}\left\|\bar{\beta}\right\|^2. \tag{50}$$

Here $\xi > 0$ and $\eta > 0$ are the coupling parameters. The coupled Eqs. (47)-(49) with Eq. (50) gives below mentioned form (time derivative of the energy functional):

$$\frac{dE}{dt} = I - D. \tag{51}$$

Here:

$$I = -\xi\langle(\bar{q}.\nabla\theta_s)\bar{\theta}\rangle - \eta\langle(\bar{q}.\nabla C_s)\bar{\beta}\rangle + \langle\bar{\theta}\,\overline{w}\rangle + \langle\bar{\beta}\,\overline{w}\rangle - \eta Sr\langle\nabla\bar{\theta}.\nabla\bar{\beta}\rangle,$$

$$D = \|\bar{q}\|^2 + \eta\left\|\nabla\bar{\beta}\right\|^2 + \xi\left\|\nabla\bar{\theta}\right\|^2. \tag{52}$$

Further, we define R_E as:

$$R_E = \max_{\mathrm{H}}\left(\frac{I}{D}\right). \tag{53}$$

Where $H = \{(\bar{q},\ \bar{\theta},\ \overline{C}\ ) \in L^2(\Omega)\colon\ \nabla.\bar{q} = 0$ and $\overline{w} = \ \bar{\theta} = \bar{C} = 0$ at $z = -\frac{1}{2}, \frac{1}{2}\}$ is the region of all permissible results to Eqs. (26)-(29), then:

$$\frac{dE}{dt} \leq\ -D(1 - R_E).$$

Implementing the classical Poincare inequality, $\|\bar{q} - \bar{q}_\Omega\|_{L^p(\Omega)} \leq \mathrm{K}\|\nabla\bar{q}\|_{L^p(\Omega)}$ $\left(\pi^2\left\|\bar{\theta}\right\|^2 \leq \left\|\nabla\bar{\theta}\right\|^2 and\ \pi^2\left\|\bar{\beta}\right\|^2 \leq \left\|\nabla\bar{\beta}\right\|^2\right)$, where Ω is an open connected compact Hausdorff space and using $\bar{q}_\Omega = \left|\frac{1}{\Omega}\right| \int_\Omega\ \bar{q}\,(\Omega)dy$, we may write:

$$\frac{dE}{dt} \leq -2\pi^2(1 - R_E)\min\left\{1, \frac{a}{Le\ \phi}\right\}E. \tag{54}$$

When $0 <\ R_E < 1$, by integrating the above inequality (54) guarantees that $E(t) \to 0$ at least exponentially as $t \to \infty$. By the fundamentals of $E(t)$, decline of θ, β follows but fails to retain the kinetic energy factor for velocity $\|\bar{q}\|^2$. Thus, the decline of $\bar{q}$ necessities to be check. Implementing the arithmetic-geometric mean in Eq. (47) yields:

$$\|\bar{q}\|^2 \leq 2\left(\left\|\bar{\theta}\right\|^2 + \left\|\bar{\beta}\right\|^2\right). \tag{55}$$

From the Eq. (47) and the above inequality (55) ensures the decline of $\bar{q}$ is understood by the decline of $E(t)$ (since $\left\|\bar{\theta}\right\|^2$ and $\left\|\bar{\beta}\right\|^2 \to 0$ as $t \to \infty$). Thus, for $R_E < 1$ considred system is stable.

However, the associated Euler-Lagrange system for R_E can be written as:

$$\xi\bar{\theta}\nabla\theta_s + \eta\bar{\beta}\nabla C_s - \left(\bar{\theta} + \bar{\beta}\right)\boldsymbol{k} + 2R_E\bar{q} = \nabla\bar{\pi}, \tag{56}$$

$$\bar{w} - \xi(\bar{q}.\nabla\theta_s) + \eta\, Sr\nabla^2\bar{\beta} + 2R_E\xi\nabla^2\bar{\theta} = 0, \tag{57}$$

$$\bar{w} - \eta(\bar{q}.\nabla C_s) + \eta\, Sr\nabla^2\bar{\theta} + 2R_E\eta\nabla^2\bar{\beta} = 0. \tag{58}$$

Here $\bar{\pi}$ is the Lagrange's multiplier. While generating the Eqs. (56)-(59), authors adopt $\chi = \left(\bar{q},\ \bar{\beta},\ \bar{\theta}\right)$ and $\mathcal{L} = I - R_E D$. Thus, the resultant Euler-Lagrange system is shown below:

$$\nabla_{\chi_i}\mathcal{L} - \frac{\partial}{\partial x_j}\nabla_{\chi_i} \circ \mathcal{L} = 0 \qquad for\ i = 1,2,3; \qquad j = 1,2,3 \tag{59}$$

Here $'\circ'$ denotes differentiation with respect to z. Now we consider R_z as the eigenvalue and estimate the maximum variation of R_z with the optimal choice of ξ and η. From the equations (56)-(59), one arrives at the following derivative expressions:

$$\frac{\partial R_z}{\partial \xi} = \frac{R_E(1-\xi R_z)\left\|\nabla\bar{\theta}\right\|^2 + \langle\tilde{B}\bar{w}\bar{\theta}\rangle - \eta R_z Sr\langle\nabla\bar{\theta}.\nabla\bar{\beta}\rangle - \psi_R}{\xi^2\left(2R_E\left\|\nabla\bar{\theta}\right\|^2 + \langle\tilde{B}\bar{w}\bar{\theta}\rangle + \xi^{-1}\eta Sr\langle\nabla\bar{\theta}.\nabla\bar{\beta}\rangle - \psi_R\right)}, \tag{60}$$

$$\frac{\partial R_z}{\partial \eta} = \frac{2(1+\xi R_z)\left[R_E(1-\eta S_z)\left\|\nabla\bar{\beta}\right\|^2 + \frac{Sr}{2}(1-\eta S_z)\langle\nabla\bar{\theta}.\nabla\bar{\beta}\rangle + \langle\tilde{A}\bar{w}\bar{\beta}\rangle - \psi_C\right]}{\xi^2(1+\eta S_z)\left[2R_E\left\|\nabla\bar{\theta}\right\|^2 + \langle\tilde{B}\bar{w}\bar{\theta}\rangle + \eta\xi^{-1}Sr\langle\nabla\bar{\theta}.\nabla\bar{\beta}\rangle - \psi_R\right]}. \tag{61}$$

Here:

$$\psi_R = R_x\langle\bar{u}\cdot\bar{\theta}\rangle + R_y\langle\bar{v}\cdot\bar{\theta}\rangle, \tag{62}$$

$$\psi_C = C_x\langle\bar{u}\cdot\bar{\beta}\rangle + C_y\langle\bar{v}\cdot\bar{\beta}\rangle.$$

Also note that if $C_x = C_y = 0,\ R_x = R_y = 0,\ Q = 0$ (vanishing heat source) and $Sr = 0$ (negligible Soret effect), then Eqns. (60)-(61) contract to:

$$\frac{\partial R_z}{\partial \xi} = \frac{(1-\xi R_z)}{2\xi^2}, \tag{63}$$

$$\frac{\partial R_z}{\partial \eta} = \frac{(1+\xi R_z)(1-\eta C_z)\left\|\nabla\bar{\beta}\right\|^2}{\xi^2(1+\eta C_z)\left\|\nabla\bar{\theta}\right\|^2}. \tag{64}$$

The coupling parameters ξ, η can be computed from the above equations as:

$$\xi = \frac{1}{R_z}\ ,\ \eta = \frac{1}{C_z} \tag{65}$$

These parameters are explored in [36]. The Eqs. (56)-(58) are evaluated for $R_E = 1$. The numerical solution involves the curl curl of Eq. (56) with 3rd component and which gives:

$$\xi R_x \frac{\partial^2\overline{\theta}}{\partial x\partial z} + \xi R_y \frac{\partial^2\overline{\theta}}{\partial y\partial z} + \xi\nabla_1^2\left[\left(-R_z + \tilde{B}\right)\bar{\theta}\right] + \eta C_x \frac{\partial^2\overline{\beta}}{\partial x\partial z} + \eta C_y \frac{\partial^2\overline{\beta}}{\partial y\partial z} + 2\nabla_1^2\overline{w} + \eta\nabla_1^2\left[\left(-C_z + \tilde{A}\right)\bar{\beta}\right] - \nabla_1^2\left(\bar{\theta} + \bar{\beta}\right) - 2\left(\frac{\partial^2\overline{u}}{\partial x\partial z} + \frac{\partial^2\overline{v}}{\partial y\partial z}\right) = 0, \tag{66}$$

Where $\nabla_1^2 = \left(\frac{\partial^2}{\partial x^2} + \frac{\partial^2}{\partial y^2}\right)$ is the Laplacian differential operator. Applying normal modes:

$$\left[\bar{q}, \bar{\beta}, \bar{\theta}, \bar{\pi}\,\right] = [q(z), \beta(z), \theta(z), \pi(z)]exp\big(i(kx + ly)\big). \tag{67}$$

Setting $\left(C_x, C_y\right)\cdot(k,l) = 0$; $\left(R_x, R_y\right)\cdot(k,l) = 0$, in Eqs. (56)-(58) and eliminating u, v and π , the required eigenvalue problem can be derived:

$$D^2w = \alpha^2 w + \alpha^2\eta h_1\beta + \alpha^2\xi h_2\theta, \tag{68}$$

$$D^2\theta = \frac{1}{(1-h_7h_8)}[(h_2 - h_1h_7)w + (h_3 - \alpha^2h_7h_8 + h_6h_7)\theta + (\alpha^2h_7 - h_4 - h_5h_7)\beta], \tag{69}$$

$$D^2\beta = \frac{1}{(1-h_7h_8)}[(h_1 - h_2h_8)w + (\alpha^2h_8 - h_6 - h_3h_8)\theta + (h_5 - \alpha^2h_7h_8 + h_4h_8)\beta]. \tag{70}$$

In Eqns. (68)-(70) the following algebraic expressions are featured:

$$h_1 = \frac{1}{2}\left[-C_z + \tilde{A} - \eta^{-1}\right], \qquad h_2 = \frac{1}{2}[-R_z + \tilde{B} - \xi^{-1}], \qquad h_3 = \alpha^2 - \frac{\xi}{4}\left(R_x^2 + R_y^2\right),$$

$$h_4 = \frac{\eta}{4}\left(C_xR_x + C_yR_y\right), \qquad h_5 = \alpha^2 - \frac{\eta}{4}\left(C_x^2 + C_y^2\right), \qquad h_6 = \frac{\xi}{4}\left(C_xR_x + C_yR_y\right),$$

$$h_7 = \frac{\eta}{2\xi}Sr, \qquad h_8 = \frac{Sr}{2}. \tag{71}$$

The associated boundary conditions are:

$$w = \beta = \theta = 0 \qquad \text{at} \qquad z = \pm\frac{1}{2} \tag{72}$$

The critical thermal Rayleigh number is:

$$R_z = max_\xi max_\eta min_\alpha\big(\xi, \eta, \alpha, Q, M, Sr, Le, R_x, R_y, C_x, C_y, C_z\big). \tag{73}$$

Numerical solutions for both the linear and non-linear stability eigenvalue problems derived are obtained next.

7. Numerical solution scheme

Computational solutions of nonlinear and linear stability eigenvalue problems are achieved with numerical Runge-Kutta methods within the MATLAB symbolic environment. Here, the BVP is first converted into an IVP. Author, split $w(z)$, $\beta(z)$ and $\theta(z)$ into real and imaginary parts. Then, the corresponding boundary conditions on $Re\big(w(z)\big)$, $Im\big(w(z)\big)$,

$Re(\beta(z)), Im(\beta(z)), Re(\theta(z))$ and $Im(\theta(z))$ is replaced with the corresponding set of initial conditions.

$$Re(w(0)) = 0,\ \ Re(Dw(0)) = 1,\ \ Im(w(0)) = 0,\ \ Im(Dw(0)) = \eta_1, \tag{74}$$

$$Re(\beta(0)) = 0,\ \ Re(D\beta(0)) = \eta_2,\quad Im(\beta(0)) = 0,\quad Im(D\beta(0)) = \eta_3, \tag{75}$$

$$Re(\theta(0)) = 0,\quad Re(D\theta(0)) = \eta_4,\quad Im(\theta(0)) = 0,\quad Im(D\theta(0)) = \eta_5. \tag{76}$$

In Eq. (76) the additional condition on $Re(Dw(0)) = 1$ is used as uncertain scale term of the outcome (z). The numericals of $\eta_1, \eta_2, \eta_3, \eta_4$ and η_5 either a real or complex numbers. The reduced system of ODE's is solved efficiently with the explicit Runge-Kutta scheme.

8. Results and discussion

In earlier sections, linear and non-linear stability discussion is presented to evaluate the impact of Soret, mass flow and inside thermal generation effects over dual diffusion Hadley-Prats transport through isotropic flat permeable channel. The bench mark outcomes of [10, 20, 21 33, 34, 44] gives the method of solving developed eigenvalue problems. In both the cases, R_z is considered to be an eigenvalue of the stability problem i. e. critical parameter. An ideal Fourier scheme is deployed to discuss the temperature instability in Hadley-Prats motion. For the variable α, the critical R_z is evaluated with $\alpha = (k; l; 0)$.

Nield [10, 20, 21, 33, 34, 44] discussed the stationary convection transport process with $\sigma = 0$. Wherein a non-oscillatory longitudinal scheme was chosen for Hadley-Prats motion with $k = 0$. Therefore, following the literature [10, 20, 21, 33, 34, 44], the results published here are for $k = 0$ and $\sigma = 0$. In the calculations, $C_z > 0$ implies that mass diffusion on upper plate is greater than on the lower plate, and $C_z < 0$ indicates the opposite scenario. In the current analysis, parameter data is prescribed as $\frac{\phi}{a} = 1$, $R_y = C_y = 0$ and $Le = 10$ which corresponds physically to a wide range of applications of experiments with salt or sugar diffusing species, the former being of direct relevance to brine-geothermal systems.

Table 1. Critical R_z at $R_x = R_y = C_x = C_y = 0,\ Q = 0, M = 0, Sr = 1$ and $Le = 10$, for the case of linear stability analysis.

$\boldsymbol{C_z}$	$\boldsymbol{R_z}$	$\boldsymbol{\alpha}$
-7	27.6937	2.01000

-6	23.719534	2.01000
-5	19.745657	2.0100
-4	15.775806	2.0100
-3	11.812646	2.0100
2	8.056467	2.4999
3	12.081960	2.4999
5	20.103332	2.4999
6	24.106080	2.4999
7	28.0842	2.4999

Table 2. Critical R_z at $R_x = R_y = C_x = C_y = 0,\ Q = 0, M = 0, Sr = 0.2$ and $Le = 10,$ for the case of non-linear stability theory.

$\boldsymbol{C_z}$	$\boldsymbol{R_z}$	$\boldsymbol{\alpha}$
-7	75.054580	1.8
-6	73.804582	1.8
-5	72.554584	1.8
-4	71.304586	1.8
-3	70.054589	1.8
-2	68.804588	1.8
2	63.8046	1.8
3	62.554565	1.8
4	61.304575	1.8
5	60.054591	1.8
6	58.804604	1.8
7	57.554577	1.8

Table 1 documents the computations for critical thermal Rayleigh number R_z with $R_x = R_y = C_x = C_y = 0,\ Q = 0, Sr = 1, M = 0$ and $Le = 10,$ for different values of the solutal z-direction Rayleigh number C_z. The results produced for these parameters correlate exactly with the earlier special case considered by Guo and Kaloni [36] and Matta *et al.* [18] wherein both mass flow ($M = 0$) and heat generation ($Q = 0$) effects were ignored. It is clear from **Table 1**, that by enhancing C_z from negative values, the R_z value decreases. However, once C_z becomes positive the value of R_z increases. Recalling the mathematical definitions of

these parameters from Eq. (12), viz, $R_z = \frac{\rho_0 g \gamma_\theta K d \Delta\theta}{\mu \alpha_m}$ and $C_z = \frac{\rho_0 g \gamma_C K d \Delta C}{\mu D_m}$, both Rayleigh numbers express respectively the ratio of thermal buoyancy force or solutal buoyancy force to the viscous hydrodynamic force. For negative C_z the solutal buoyancy force opposes the motion whereas for positive C_z it assists the motion. At large negative C_z the counteraction is strongest and it is progressively diminished as C_z becomes less negative. This accelerates the onset of thermal instability and decreases the critical thermal Rayleigh number R_z. The reverse effect is induced with higher positive values of C_z which serve to stabilize the regime and thereby enhance the critical thermal Rayleigh number, R_z, which corresponds to a delay in the onset of instability. With the modification in both polarity and magnitude of the solutal *z*-direction Rayleigh number C_z, both the direction and size of the solutal buoyancy force is modified. This naturally will induce variations in the solute concentration and will also manifest in depletion in temperature at the lower boundary. Fluid mixing will also be strongly modified in the porous regime. The interplay between thermal and species diffusion fields will be significantly altered and stability of the system will undergo marked changes. Hence the relative contributions of vertical thermal and solutal Rayleigh numbers are very prominent mechanisms which can be manipulated to regulate the regime circulation characteristics. Furthermore, even though these solutions are evaluated by solving the eigenvalue problem encountered from the linear stability theory by neglecting the non-linear terms in the perturbation equations, the influence is still considerable on the interaction of thermal and mass diffusion fields and effectively the stability of the entire regime.

Table 2 summarizes the computations for R_z at $R_x = R_y = C_x = C_y = 0$, $Q = 0, Sr = 0.2, M = 0$ and $Le = 10$, with different values of C_z. In this case, the Soret number is five times smaller than that in Table 1 (where $Sr = 1$), whereas all other parameters are identical including $Le = 10$ (thermal diffusion rate is ten times the solute diffusion rate). **Table 2** demonstrates that increasing C_z from negative values to positive values, again R_z value is decreased implying a faster onset of thermal instability i. e. more rapid attainment of destabilization of the fluid flow. However, while the trend is the same but significant difference in magnitude of critical thermal Rayleigh parameter. For example, when C_z = -7, with *Sr* = 1 (**Table 1**), a much lower R_z of 26.6937 is computed when *Sr* = 0.2 (Table 2), which gives R_z of 75.054580. The implication is that when Soret thermo-diffusion effect is suppressed the onset of instability is delayed significantly and the stability of the regime is enhanced. As elaborated earlier, the Soret effect involves the concentration distribution being modified by temperature gradient. Physically higher values of Soret number correspond to higher temperature gradient which results in higher convective flow. This serves to destabilize the regime. Weaker Soret effect is therefore conducive to achieving enhanced thermo-solutal stability. This behaviour is confirmed if we examine the opposite case of C_z =+7, in both Tables 1 and 2. When *Sr* = 1 (**Table 1**) the computations give R_z of 28.0842 whereas when *Sr* = 0.2 (Table 2) the critical thermal Rayleigh number is massively increased again to R_z of 57.554577. In other words, the threshold for destabilization is massively increased with a decrement in Soret number. It is also interesting to note that **Table 1** gives significantly higher values of the wave number (α) which is consistently in excess of 2, whereas for Table 1 it is always less than 2. Overall Table 1 and 2 demonstrate that higher values of the vertical solutal Rayleigh number and Soret number substantially contribute to inducing flow instability in the porous medium system. The inclusion of thermos-diffusive effects, in particular, which has been neglected in many previous studies, is strongly justified for achieving more physically realistic and accurate geothermal simulations.

Figure 2 depicts the variations in R_z with C_z at $R_x = C_x = R_y = C_y = 0,\ M = 0,\ Q = 0,\ Le = 10$ (for the non-linear stability case) with a range of Soret number values (Sr) with mass flow and internal heat generation neglected. The deviations of R_z with C_z are noteworthy. The value R_z has a decreasing trend for the negative values of C_z whereas it has an increasing trend for the positive values of C_z. This pattern implies that for negative values of C_z the non-linear stability of the fluid system is elevated; albeit gradually as the threshold for reaching the critical Rayleigh number is reduced. The system hydro-thermo-solutal stability is elevated by increasing the value of C_z. This indicates that to sustain higher thresholds for instability to be initiated the solutal Rayleigh number should be positive and the Soret number should be minimal. In all the plots a sustained symmetric topology is computed, and the nonlinearity is clearly captured in the inverse parabolic distributions.

Figure 3 shows the evolution in R_z with C_z at $R_x = C_x = R_y = C_y = 0,\ M = 0,\ Q = 0,\ Le = 10$ (for the linear stability case) again for various Soret number values *(Sr)* with mass flow *(M = 0)* and internal heat generation *(Q = 0)* neglected. The profiles of R_z with C_z are clearly linear. The stability of the fluid system is clearly decreasing i. e. the threshold for the onset of instability is reduced (lower critical thermal Rayleigh number) with increasing C_z. There is no switch in behaviour as computed for the nonlinear stability analysis (the trough in Fig. 3 marks the point of the behaviour reversing).

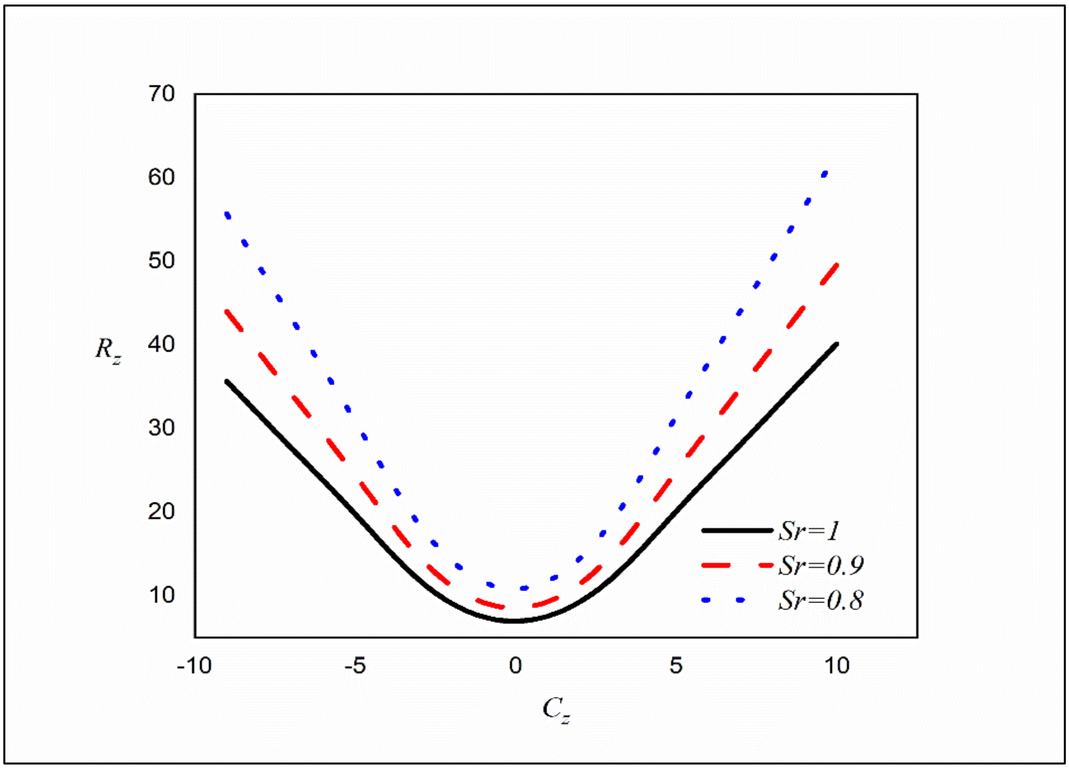

Figure 2. R_z versus C_z at $R_x = C_x = R_y = C_y = 0,\ M = 0,\ Q = 0,\ Le = 10$ (for the non-linear stability analysis).

Increasing Soret number again serves to accelerate the onset of instability, however much lower values are required to compute this change (*Sr* = 0.001, 0.1, 0.2) relative to the nonlinear stability solution (Fig. 2) where *Sr* =0.8, 0.9 and 1.0. Additionally higher values of R_z are computed for the linear stability analysis in Figure 3 (peak values approach 80 and minimal values still exceed 40) compared with the nonlinear stability simulations of Figure 2 (where peak values do not exceed 60 and minimal values struggle to exceed 10).

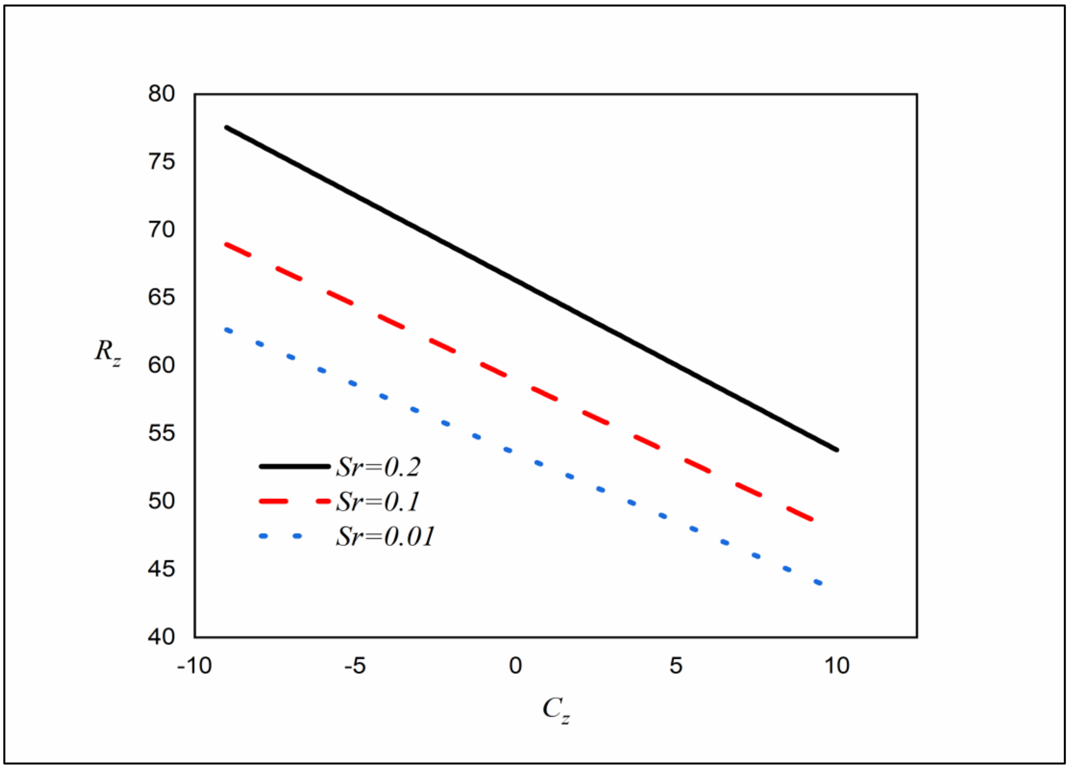

Figure 3. Variations of R_z with C_z at $R_x = C_x = R_y = C_y = 0,\ M = 0,\ Q = 0,\ Le = 10$ (for the linear stability case).

Table 3. Critical R_z at $R_x = R_y = C_x = C_y = 0,\ Q = 0, M = 0, C_z = 5$ and $Le = 10$, for the case of non-linear stability analysis.

$Sr = 1.0$	R_z	20.10091	20.113278	20.106350	20.080269	20.097005
	α	1	1.25	1.5	1.75	2
$Sr = 0.9$	R_z	24.847325	24.850023	24.858142	24.851304	24.853505
	α	1	1.25	1.5	1.75	2
$Sr = 0.8$	R_z	31.457275	31.475334	31.488788	31.483281	31.491139
	α	1	1.25	1.5	1.75	2

Table 3 shows the differences in the critical R_z with $R_x = R_y = C_x = C_y = 0,\ Q = 0, M = 0, C_z = 5$ and $Le = 10$, for non-linear case of stability, with various Soret parameter and wave number values. It is apparent that there is a linear deviation of R_z with wave number. For decreasing Soret numbers, there is still deviation of R_z with wave number of a linear fashion, but as noted earlier, the system is more stable since the critical thermal Rayleigh number is increased i. e. the onset of instability is delayed with weaker Soret effect. Hence, a reduction in Soret thermo-diffusive flux effect (decreasing *Sr*) serves to enhance the stability

of the porous medium regime. The corresponding tabulated solutions for **Figs. 2 and 3** are shown in **Tables 4-6** for different values of Sr. The trends computed in **Figs. 2 and 3** are confirmed in these tables.

Table 4. Critical R_z at $R_x = R_y = C_x = C_y = 0,\ Q = 0, M = 0, C_z = 5$ and $Le = 10$, for the case of linear stability theory.

$Sr = 0.2$	R_z	92.584529	72.108131	60.054591	52.650696	48.053788
	α	1	1.25	1.5	1.75	2
$Sr = 0.1$	R_z	82.297367	64.096110	53.381931	46.800605	42.714502
	α	1	1.25	1.5	1.75	2
$Sr = 0.05$	R_z	77.965914	60.722648	50.572345	44.337437	40.466325
	α	1	1.25	1.5	1.75	2

Table 5. Critical R_z at $R_x = R_y = C_x = C_y = 0,\ Q = 0, M = 0, C_z = -3$ and $Le = 10$, for the case of non-linear stability theory.

$Sr = 1.0$	R_z	11.877313	11.853390	11.836900	11.823397	11.812646
	α	1	1.25	1.5	1.75	2
$Sr = 0.9$	R_z	14.645448	14.629028	14.607716	14.588865	14.574264
	α	1	1.25	1.5	1.75	2
$Sr = 0.8$	R_z	18.5327	18.51345	18.481237	18.456782	18.435418
	α	1	1.25	1.5	1.75	2

Table 6. Critical R_z at $R_x = R_y = C_x = C_y = 0,\ Q = 0, M = 0, C_z = -3$ and $Le = 10$, for linear stability.

$Sr = 0.2$	R_z	92.997048	82.108159	70.054589	62.650590	58.053691
	α	1	1.25	1.5	1.75	2
$Sr = 0.1$	R_z	91.186271	72.985044	62.270764	55.689494	51.603358
	α	1	1.25	1.5	1.75	2
$Sr = 0.05$	R_z	86.386997	69.143732	58.993365	52.758464	48.887408
	α	1	1.25	1.5	1.75	2

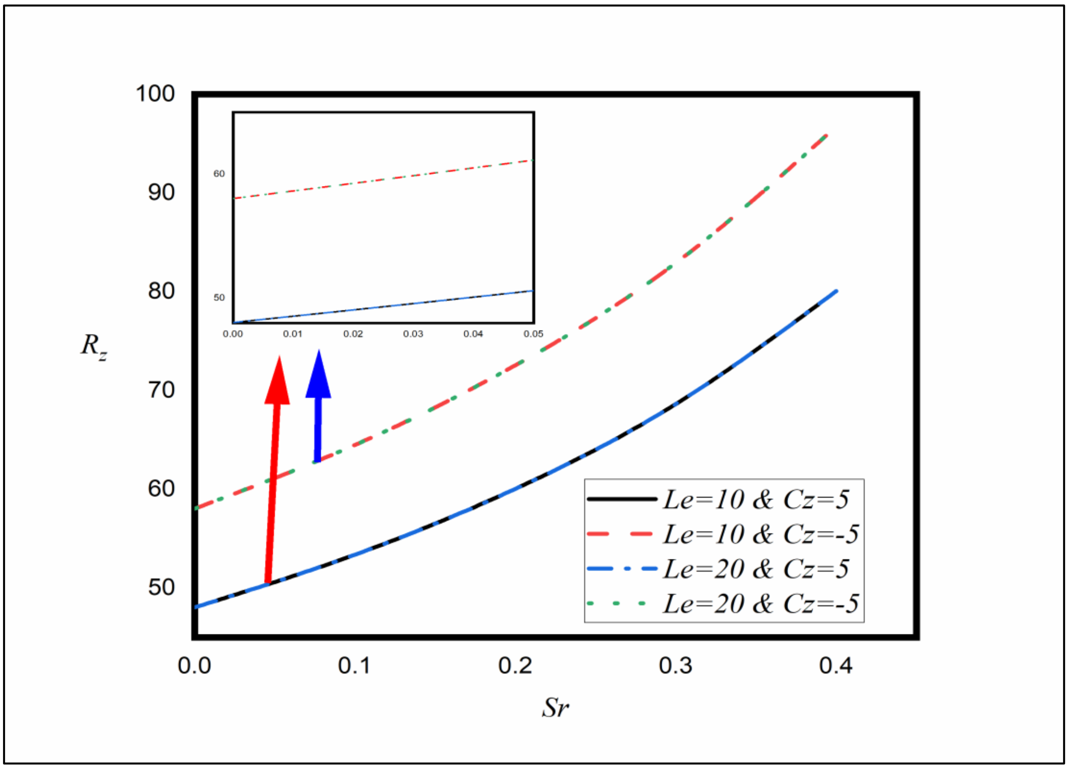

Figure 4. Deviations of R_z with Sr at $R_x = C_x = R_y = C_y = 0,\ M = 10,\ Q = 0,$ (for the linear stability case).

Figure 4 shows the modification in critical R_z with Soret parameter Sr for linear case with the collective influence of Lewis number (Le) and solutal Rayleigh number (C_z). The graph shows that when keeping the value of C_z as constant (e. g. - 5) with varying the value of Lewis number (from 10 to 20), the curves are coinciding. However, with the value C_z changed from positive to the negative then curves are not coinciding. For growing values of C_z the fluid system is more unstable. Higher Lewis number clearly reduces the critical thermal Rayleigh number, R_z significantly, indicating that a reduction in mass diffusivity relative to thermal diffusivity serves to enhance the stability of the regime. This trend is sustained at any Soret number value. Increasing Soret number however shows that critical thermal Rayleigh number, R_z is elevated and that the onset of instability is delayed.

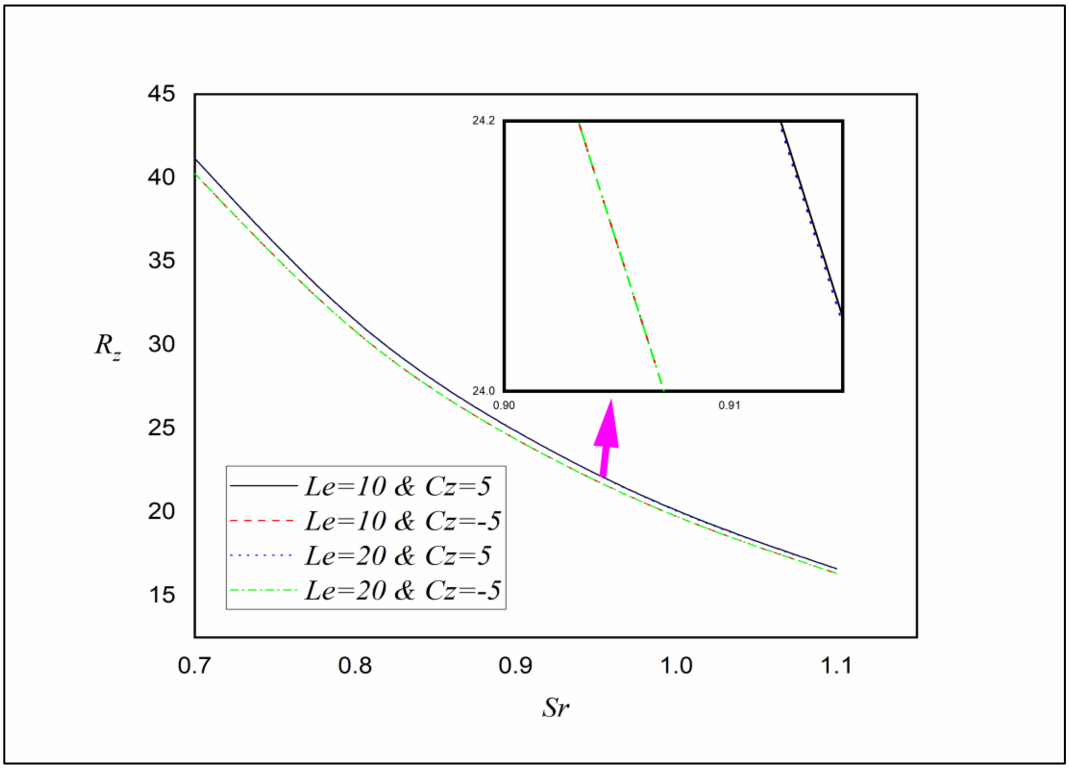

Figure 5. Variations of R_z with Sr at $R_x = C_x = R_y = C_y = 0,\ M = 10,\ Q = 0,$ (for the non-linear stability case).

Figure 5 is represented for deviations of R_z with Sr for $R_x = C_x = R_y = C_y = 0,\ M = 10,\ Q = 0$ (for the non-linear stability theory). As described in Fig. 4 for the constant C_z value case, the curves coincide also for non-linear stability of the fluid system for case of variation in Lewis number. It is clearly noted that the regime is more stable (critical Rayleigh number is enhanced) with the combined influence of Lewis number and horizontal concentration Rayleigh number. **Figure 6** is plotted for deviations of R_z with Sr for $R_x = C_x = R_y = C_y = 0,\ Le = 10,\ Q = 0$ (again for the non-linear stability case). Here the curves are drawn for the different combinations of mass flow parameter (*M*) and vertical concentration (solutal) Rayleigh number, C_z. It is interesting to note that only a very weak modification (reduction) is induced with a doubling in mass flow rate (*M* from 5 to 10) and a large switch in vertical concentration Rayleigh number (from assisting at 5 to opposing at -5). The stability of the system is therefore weakly reduced with these changes in mass flow rate and solutal Rayleigh number since critical Rayleigh number is decreased marginally. With an increase in the value of Soret parameter Sr, critical Rayleigh number is however very strongly depleted indicating that the regime becomes more unstable.

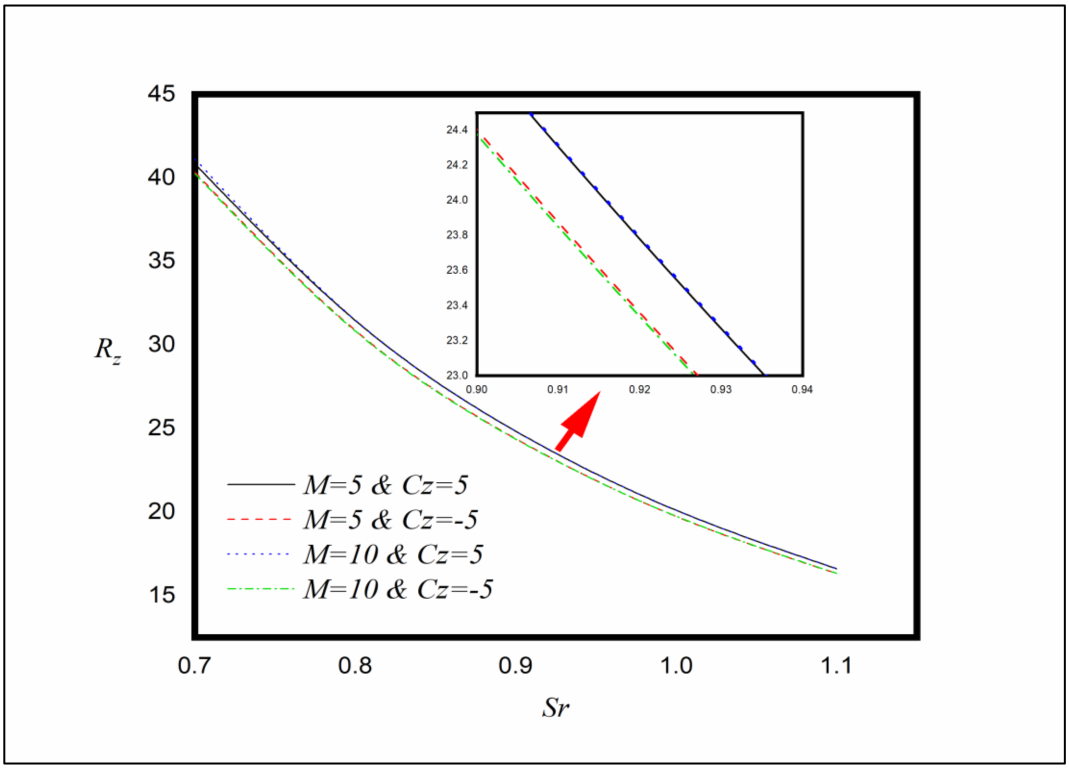

Figure 6. Variations of R_z with Sr at $R_x = C_x = R_y = C_y = 0,\ Le = 10,\ Q = 0,$ (for the non-linear stability case).

Figure 7 (linear case) demonstrates a very different trend to Fig 6- a more dramatic increase is induced in critical thermal Rayleigh number over the same numerical changes in mass flow rate and vertical solutal Rayleigh number. The threshold for instability is therefore elevated and higher mass flow rate and solutal Rayleigh number contribute to stabilizing the regime. However, the impact of Soret number (*Sr*) is essentially the same for the linear case. Continuous decrement in thermal Rayleigh parameter with an increment in Soret number, implying again that the edge for the onset of instability is reduced and the porous medium regime is rendered less stable. Overall, the combination of all physical parameters involved i. e. Lewis number, mass flow parameter, internal heat source parameter, Soret number, vertical solutal Rayleigh number for both stability cases; exert a tangible influence on the critical thermal Rayleigh numbers computed.

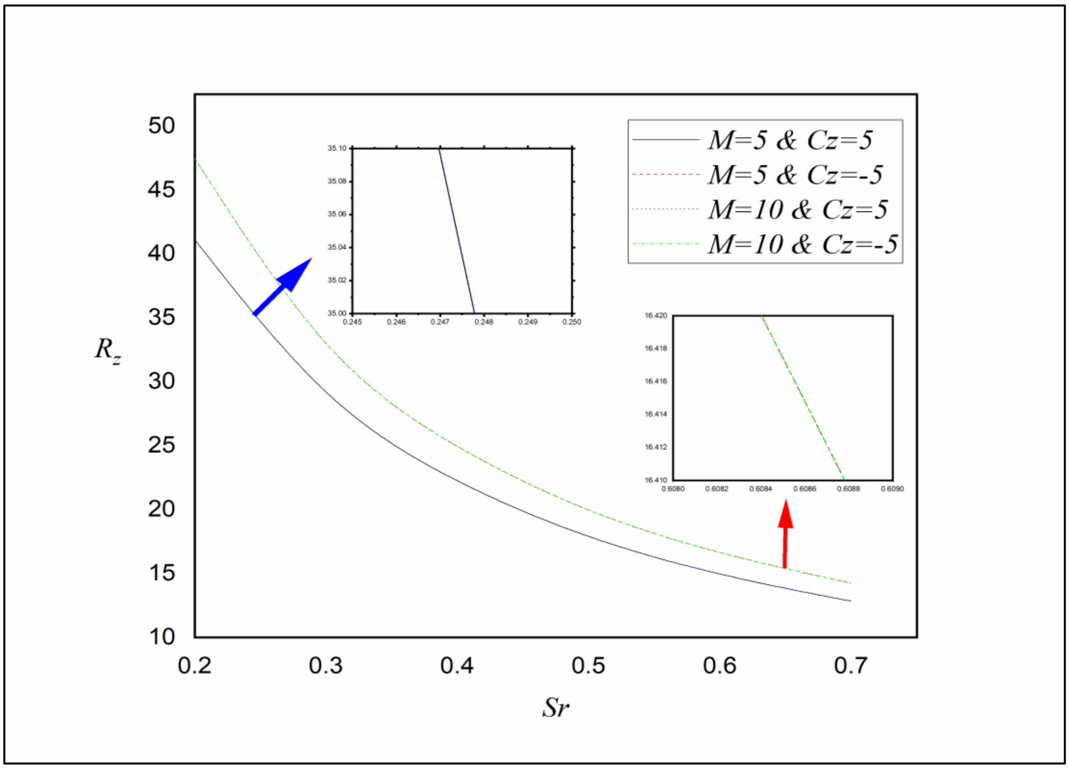

Figure 7. Deviations of R_z with Sr at $R_x = C_x = R_y = C_y = 0$, $Le = 10$, $Q = 0$, (for the linear stability case).

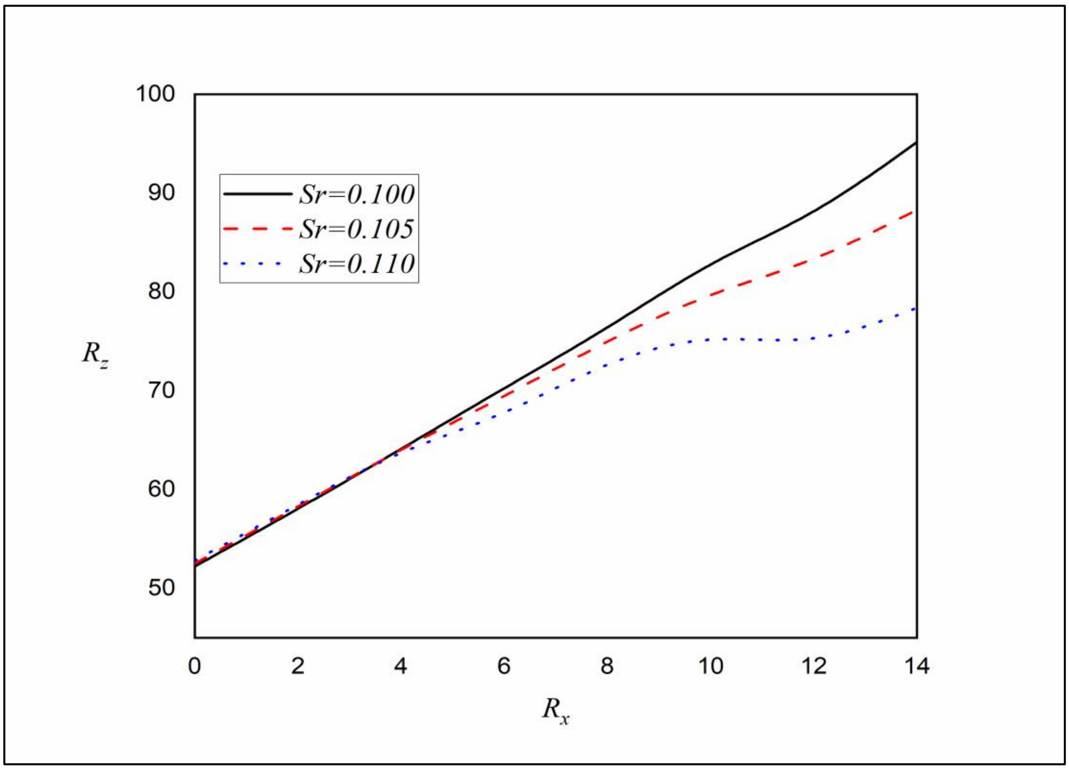

Figure 8. Deviations of R_z with R_x at $C_x = 10$, $R_y = C_y = 0$, $Q = 0, M = 0, C_z = -5$ and $Le = 10$, for the linear stability case.

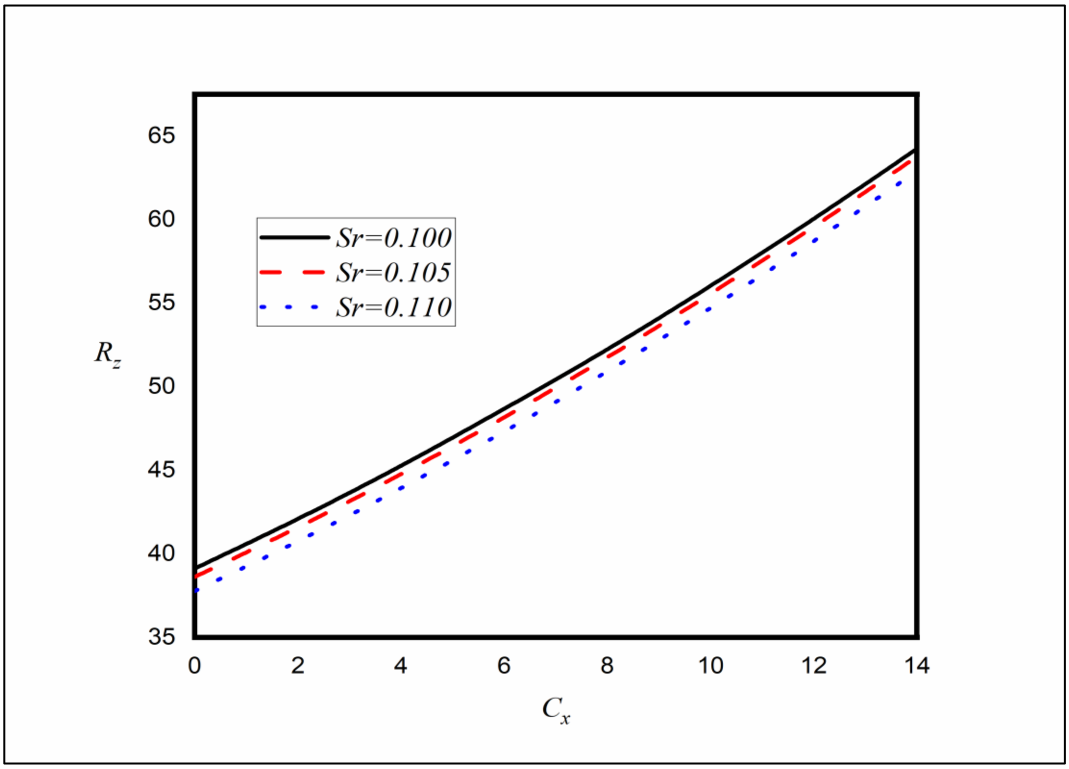

Figure 9. Deviations of R_z with C_x at $R_x = 5,\ R_y = C_y = 0,\ Q = 0, M = 0, C_z = 5$ and $Le = 10$, for the linear stability case.

Table 7 and Figure 8 show the differences in the critical R_z with R_x for $C_x = 10$, $R_y = 0,\ C_y = 0,\ Q = 0, M = 0, C_z = -5$ and $Le = 10$, for the case of linear stability, with various Soret parameter and wave number values. It is clear that for increasing the horizontal value of thermal Rayleigh number (horizontal thermal gradient), the vertical thermal Rayleigh number also increases and it causes the fluid flow through infinite porous layer to become more stable. **Table 8 and Figure 9** show the differences in the critical R_z with C_x for $R_x = 5,\ R_y = 0,\ C_y = 0,\ Q = 0, M = 0, C_z = 5$ and $Le = 10$, for the case of linear stability, with various Soret parameter and wave number values. It is observed that increasing the horizontal value of solutal Rayleigh number (horizontal solutal gradient) also increases the vertical thermal Rayleigh number and it causes the fluid flow to become more stable. Hence, in both the cases it is clear that small increment in the Soret parameter results the fluid flow through infinite porous layer which is having slightly destabilisation nature.

Table 7. Critical R_z at $C_x = 10$, $R_y = C_y = 0$, $Q = 0, M = 0, C_z = -5$ and $Le = 10$, for linear stability.

R_x	0	2	4	6	8	10	12	14
$Sr = 0.100$	52.2306	58.0780	64.1042	70.2584	76.4236	82.7681	88.1540	95.1505
$Sr = 0.105$	52.5224	58.2960	64.0138	69.4852	74.9677	79.6689	83.3642	88.3053
$Sr = 0.110$	52.8175	58.4797	63.7089	67.8189	72.6358	75.1761	75.3196	78.4032

Table 8. Critical R_z at $R_x = 5$, $R_y = C_y = 0$, $Q = 0, M = 0, C_z = 5$ and $Le = 10$, for linear stability.

C_x	0	2	4	6	8	10	12	14
$Sr = 0.100$	39.1246	42.0968	45.2685	48.6886	52.2424	56.0402	60.0385	64.2337
$Sr = 0.105$	38.6280	41.5975	44.7795	48.1711	51.7694	55.5707	59.5713	63.7671
$Sr = 0.110$	37.7888	40.7580	43.9387	47.3276	50.9214	54.7161	58.7074	62.8902

Tables 9, 10 and **11** show the consequence of simultaneous presence of thermal and solutal gradients. **Table 9** shows the differences in the critical R_z with Le for $R_x = C_x = 2$, $R_y = 0$, $C_y = 0$, $Q = 0, M = 0, C_z = 10$ and $Sr = 0.110$, for the case of linear stability, with various Lewis number and wave number values. Here, it is interestingly observed that, increasing the Lewis number firstly decreases the vertical thermal Rayleigh number up to $Le = 0.50$, after this, again the value of vertical thermal Rayleigh number increases then again it decreases. Hence, in the presence of thermal and solutal gradients the Lewis number gives the quantitative changes of stability of fluid flow in an infinite porous layer. Similarly, **Table 10** shows the differences in the critical R_z with Le for $R_x = C_x = 2$, $R_y = 2$, $C_y = 2$, $Q = 0, M = 0, C_z = 10$ and $Sr = 0.110$, for the case of non-linear stability, with various Lewis number and wave number values. This also shows the same stability nature like linear stability analysis as explained earlier in above Table 9. Hence, increasing the value of Lewis number gives a scope of both stabilisation and destabilisation trends are to be observed in the fluid flow. **Table 11** shows the differences in the critical R_z with Le for $R_x = C_x = 1$, $R_y = 1$, $C_y = 1$, $Q = 0, M = 0, C_z = 10$ and $Sr = 0.110$, for the case of non-linear stability, with various Lewis number and wave number values. The stability nature of **Table 11** is similar to the **Tables 9** and **10**.

Table 9. Critical R_z at $R_x = 2, C_x = 2$ $R_y = C_y = 0,$ $Q = 0, M = 0, C_z = 10$ and $Sr = 0.110$, for the case of linear stability.

Le	R_z	α	Le	R_z	α	Le	R_z	α
0.01	38.1260	3.3999	3.00	31.9827	3.2299	11.00	34.0015	3.1799
0.05	30.8095	3.3799	5.00	33.2902	3.1799	12.00	33.5185	3.2099
0.10	29.8862	3.3699	7.00	34.1386	3.1999	13.00	32.7090	3.3599
0.50	29.9574	3.3299	8.00	34.3716	3.1399	14.00	31.7213	3.3199
1.00	30.3971	3.2999	9.00	34.4304	3.1499	14.50	31.1641	3.3499
2.00	31.3204	3.2599	10.00	34.3271	3.1599	15.00	30.5505	3.3799

Table 10. Critical R_z at $R_x = 2, C_x = 2$ $R_y = C_y = 2,$ $Q = 0, M = 0, C_z = 10$ and $Sr = 0.10$, for the case of non-linear stability.

Le	R_z	α	Le	R_z	α	Le	R_z	α
0.01	48.0104	3.1532	5.00	30.9374	3.1262	200	25.0524	3.2065
0.05	33.0192	3.1121	10.0	32.0162	3.1262	220	17.9321	3.3277
0.10	30.9291	3.1179	50.0	36.9419	3.1982	240	10.2765	3.3975
0.50	29.9713	3.1068	100	38.3703	3.1625	245	6.9854	3.4029
1.00	29.8624	3.1056	150	34.0623	3.1623	250	4.1538	3.4176

Table 11. Critical R_z at $R_x = 1, C_x = 1$ $R_y = C_y = 1,$ $Q = 0, M = 0, C_z = 10$ and $Sr = 0.10$, for the case of non-linear stability.

Le	R_z	α	Le	R_z	α	Le	R_z	α
0.01	35.0154	3.1532	10.0	32.1167	3.1362	500	35.9469	3.2075
0.05	31.9194	3.1121	50.0	32.9419	3.1482	600	33.7894	3.2429
0.10	30.2291	3.1179	100	34.5703	3.1425	700	28.9548	3.2579
0.50	29.2713	3.1068	200	37.9624	3.1623	800	22.4292	3.2931
1.00	29.1924	3.1056	300	39.6529	3.1765	900	15.4132	3.3421
5.00	29.9379	3.1362	400	40.9428	3.1977	1000	6.54127	3.4176

Table 12 shows the differences in the critical R_z with Sr for $R_y = 0,\ C_y = 0,\ Q = 0, M = 0, C_z = 5$ and $Le = 14.5$, for the case of linear instability analysis to understand the effect of the Soret parameter as it represents the mass diffusion due to thermal gradient under the influence of inclined gradients. From the **Table 12** it is clear that in the absence of Soret parameter, the effect of inclined thermal and solutal gradients cause the fluid flow to become more unstable. Also, the Soret effect under the influence of inclined thermal and solutal gradients decreases the rate of destabilisation and finally it causes the fluid flow to become stable.

Table 12. Critical R_z at $R_y = C_y = 0,\ Q = 0, M = 0, C_z = 5$ and $Le = 14.5$, for the case of linear stability.

Sr	R_z	R_z	R_z	R_z	R_z
	R_x & $C_x = 0$	R_x & $C_x = 1$	R_x & $C_x = 2$	R_x & $C_x = 3$	R_x & $C_x = 4$
0	34.4784	33.6818	31.3962	26.3258	19.2422
0.01	34.8266	34.3853	32.8029	29.2384	24.8595
0.02	35.1820	35.0668	34.2011	31.5972	29.0357
0.03	35.5447	35.6388	35.7413	35.0227	33.7085
0.04	35.9149	36.1799	36.7460	37.7217	38.6242
0.05	36.2930	36.6877	37.8172	39.5860	41.7629
0.06	36.6791	37.1423	38.5254	40.8208	44.0027
0.07	37.0735	37.5416	38.9366	41.2488	44.4603
0.08	37.4765	37.8793	39.0208	40.8539	43.1483
0.09	37.8883	38.1318	38.7584	39.3408	40.4871
0.10	38.3093	38.3175	38.9456	39.6381	39.7094

9. Conclusions

Motivated by applications in geothermal systems and industrial materials manufacturing processes, a numerical scheme is devised to examine the thermo-solutal convective instability in the horizontal isotropic, homogenous porous material under the impact of inside thermal generation, mass diffusion, thermo-diffusion, horizontal temperature and solutal gradient effects. Both linear and non-linear stability analyses have been conducted. The critical values of R_z (thermal vertical Rayleigh number) have been evaluated with the aid of numerical shooting quadrature for various emerged unite-less numbers. However, the central findings are listed below under limiting sense:

(i) For the linear stability case, a significant increase is induced in critical thermal Rayleigh number with elevation in mass flow rate and vertical solutal Rayleigh number. The threshold for instability is therefore elevated and higher mass flow rate and solutal Rayleigh number contribute to stabilizing the regime. For the nonlinear stability case, however the opposite trend is computed and increasing mass flow rate and vertical solutal Rayleigh number cause a decline in critical thermal Rayleigh parameter and thus, reduce the stability.

(ii) With growing Soret parameter (*Sr*), the linear and nonlinear stability study show that there is a decline in critical thermal Rayleigh parameter and thus, the onset of instability is reduced, and the porous medium regime is rendered less stable.

(iii) An elevation in Lewis number significantly decreases the critical thermal Rayleigh number, R_z significantly at any Soret number, indicating that a reduction in mass diffusivity relative to thermal diffusivity serves to enhance the stability of the regime.

(iv) Critical thermal Rayleigh number exhibits a linear decay with wave number, even for the nonlinear stability analysis.

(v) With decreasing Soret numbers, for the linear stability analysis, still a linear decline in critical thermal Rayleigh parameter with wave number; however the system is more stable since the critical thermal Rayleigh number is increased i. e. the onset of instability is delayed with weaker Soret effect.

(vi) Substantially greater magnitudes of critical thermal Rayleigh number are computed for the linear stability study and validated with the nonlinear stability discussion at any value of Soret number.

(vii) Negative vertical solutal Rayleigh number $,C_z$ accelerate the onset of thermal instability and decrease the critical thermal Rayleigh number, R_z. The reverse effect is induced with higher positive values of C_z which serve to stabilize the regime and thereby enhance the critical thermal Rayleigh number, R_z, which corresponds to a delay in the onset of instability.

(viii) With the modification in both polarity and magnitude of the solutal Rayleigh number C_z, both the direction and size of the solutal buoyancy force is modified and the stability of the regime is strongly influenced.

(ix) It is clear that for increasing the horizontal value of thermal Rayleigh number (horizontal thermal gradient), the vertical thermal Rayleigh number also increases and it causes the fluid flow through infinite porous layer to become more stable. It is also observed that increasing the horizontal value of solutal Rayleigh number (horizontal solutal gradient), the vertical thermal Rayleigh number also increases and it causes the fluid flow to become more stable. Hence, in both the cases it is clear that small increment in the Soret parameter results the fluid flow which is having slightly destabilisation nature.

(x) The Soret effect under the influence of inclined thermal and solutal gradients decreases the rate of destabilisation and it causes the fluid flow to become stable.

The present investigation has identified some interesting features of both linear and nonlinear stability in double diffusion Hadley-Prats under the action of porous medium, internal heat source, mass flow and Soret thermo-diffusion with thermal convection conditions. However, attention has been confined to Newtonian fluids and the Darcy model. Future studies may address non-Newtonian e. g. couple stress nanofluids and non-Darcy inertial effects. Furthermore, rotational body force effects and viscous dissipation [44] have also been ignored, both of which are relevant to geothermal energy systems. These constitute interesting pathways for future simulations and will be communicated imminently.

Acknowledgements:

The author wishes to express his gratitude to the Reviewers who highlighted important areas for improvement in the earlier draft of this article. Their suggestions have served specifically to enhance the clarity and depth of the interpretation of results in the revised manuscript.

References

[1] F. Chen, “Convective instability in superposed fluid and anisotropic porous layers,” *Phys. Fluids A: Fluid Dynamics.*, vol. 3, pp. 556-565, 1991. DOI: 10.1063/1.858117.

[2] G. Bendrichi and L. W. Shemilt, “Mass transfer in horizontal flow channels with thermal gradients,” *Can. J. Chem Eng.*, vol. 75, pp. 1067-1074, 1997. DOI: 10.1002/cjce.5450750609

[3] B. Straughan, “Nonlinear stability for thermal convection in a Brinkman porous material with viscous dissipation,” *Transp. Porous Media.*, vol. 134, pp. 303-314, 2020. DOI: 10.1007/s11242-020-01446-5.

[4] J. D. Anderson, R. E. Bollinger and D. E. Lamb, “Gas phase controlled mass transfer in two-phase annular horizontal flow,” *AIChE. Journal.*, vol. 10, pp. 640-645, 1964. DOI: 10.1002/aic.690100513.

[5] M. E. Taslim and U. Narusawa, “Thermal stability of horizontally superposed porous and fluid layers,” *J. Heat Transf.*, vol. 111, pp. 357-62, 1989. DOI: 10.1115/1.3250685.

[6] N. Deepika, and P. A. L. Narayana, “Effects of vertical throughflow and variable gravity on Hadley–Prats flow in a porous medium”, *Transp. Porous Media*, vol. 109, pp. 455–468, 2015. DOI: 10.1007/s11242-015-0528-3.

[7] N. Deepika, A. Matta and P. A. L. Narayana, “Effect of throughflow on double diffusive convection in a porous medium with concentration based internal heat source”, *Journal of porous media*, vol. 19, pp. 1-10, 2016. DOI**:** 10.1615/JPorMedia.v19.i4.20.

[8] C. W. Horton and F. T. Rogers, “Convection currents in a porous medium,” *J. Appl. Physics.*, vol. 16, pp. 367-370, 1945. DOI: 10.1063/1.1707601.

[9] E. R. Lapwood, “Convection of a fluid in a porous medium,” *Proc. Cambridge Phil. Soc.*, vol. 44, pp. 508-521, 1948. DOI: 10.1017/S030500410002452X.

[10] D. A. Nield, “Convection in a porous medium with inclined temperature gradient: additional results,” *Int. J. Heat and Mass Transf.*, vol. 37, pp. 3021-3025, 1994. DOI: 10.1016/0017-9310(94)90356-5.

[11] A. Barletta, M. Celli and D. A. Nield, “Unstable buoyant flow in an inclined porous layer with an internal heat source,” *Int. J. Therm. Sci*, vol. 79, pp. 176-182, 2014. DOI: 10.1016/j.ijthermalsci.2014.01.002.

[12] D. A. Nield and A. Bejan, “*Convection in Porous Media*,” 4th edition, Springer, Berlin, 2013.

[13] A. A. Hill, “Double-diffusive convection in a porous medium with a concentration based internal heat source,” *Proc. R. Soc. A.*, vol. 461, pp. 561-574, 2005. DOI: 10.1098/rspa.2004.1328.

[14] J. E. Weber, “Convection in a porous medium with horizontal and vertical temperature gradients,” *Int. J. Heat Mass Transf.,* vol. 17, pp. 241-248, 1974. DOI: 10.1016/0017-9310(74)90085-4.

[15] D. B. Ingham and I. Pop, “*Transport Phenomena in Porous Media*,” Pergamon press, UK, 1998.

[16] K. Vafai, “*Handbook of Porous Media*,” 2nd Edt, CRC Press, Boca Raton, USA, 2005.

[17] D. A. Nield, D. M. Manole and J. L. Lage, “Convection induced by inclined thermal and solutal gradients in a shallow horizontal layer of a porous medium,” *J. Fluid Mech.,* vol. 257, pp. 559-574, 1993. DOI: 10.1017/S0022112093003209.

[18] D. M. Manole, J. L. Lage and D. A. Nield, “Convection induced by inclined thermal and solutal gradients, with horizontal mass flow, in a shallow horizontal layer of a porous medium,” *Int. J. Heat Mass Transfer,* vol. 37, pp. 2047-2057, 1994. DOI: 10.1016/0017-9310(94)90306-9.

[19] A. Barletta and D. A. Nield, “Instability of Hadley-Prats flow with viscous heating in a horizontal porous layer,” *Transp. Porous Media.,* vol. 84, pp. 241-256, 2010. DOI: 10.1007/s11242-009-9494-y.

[20] A. Matta, P. A. L. Narayana and A. A. Hill, “Double diffusive Hadley-Prats flow in a horizontal porous layer with a concentration based internal heat source,” *J. Math. Anal. Appl.,* vol. 452, pp. 1005-1018, 2017. DOI: 10.1016/j.jmaa.2017.03.039.

[21] A. Matta, P. A. L. Narayana and A. A. Hill, “Double diffusive Hadley-Prats flow in a porous medium subject to gravitational variation,” *Int. J. Thermal Sci.,* vol. 102, pp. 300-307, 2016. DOI: 10.1016/j.ijthermalsci.2015.10.034.

[22] A. Barletta, M. Celli and D. A. S. Rees, “The onset of convection in a porous layer induced by viscous dissipation: A linear stability analysis,” *Int. J. Heat Mass Transf.,* vol. 52, pp. 337-344, 2009. DOI: 10.1016/j.ijheatmasstransfer.2008.06.001.

[23] R. Thirlby, “Convection in an internally heated layer,” *J. Fluid Mech.,* vol. 44, pp. 673-693, 1970. DOI: 10.1017/S0022112070002082.

[24] W. Schwiderskei and J. A. Schwabh, “Convection experiments with electrolytically heated fluid layers,” *J. Fluid Mech.,* vol. 48, pp. 703-719, 1971. DOI: 10.1017/S0022112071001812.

[25] D. J. Tritton and M. N. Zarraga, "Convection in horizontal layers with internal heat generation: Experiments," *J. Fluid Mech.*, vol. 30, pp. 21-31, 1967. DOI: 10.1017/S0022112067001272.

[26] C. Parthiban and P. R. Patil, "Effect of non-uniform boundary temperatures on thermal instability in a porous medium with internal heat source," *Int. Commun. Heat Mass Transfer*, vol. 22, pp. 683-692, 1995. DOI: 10.1016/0735-1933(95)00054-3.

[27] C. Parthiban and P. R. Patil, "Thermal instability in an anisotropic porous medium with internal heat source and inclined temperature gradient," *Int. Commum. Heat Mass Transfer*, vol. 24, pp. 1049-1058, 1997. DOI: 10.1016/S0735-1933(97)00090-0.

[28] J. Guo, and P. N. Kaloni, "Nonlinear stability and convection induced by inclined thermal and solutal gradients," *Z Angew Math Phys.*, vol. 46, pp. 645-654, 1995. DOI: 10.1007/BF00949071.

[29] P.N. Kaloni and Z. Qiao, "Non-linear stability of convection in a porous medium with inclined temperature gradient". *Int. J. Heat Mass Transf*. 40, 1611–1615, 1997. DOI: 10.1016/S0017-9310(96)00204-9.

[30] P.N. Kaloni and Z. Qiao, "Nonlinear convection induced by inclined thermal and solutal gradients with mass flow". *Contin. Mech. Thermodyn*. 12, 185–194, 2000. DOI: 10.1007/s001610050134.

[31] P.N. Kaloni and Z. Qiao, "Non-linear convection in a porous medium with inclined temperature gradient and variable gravity effects". *Int. J. Heat Mass Transf*. 44, 1585–1591, 2001. DOI: 10.1016/S0017-9310(00)00196-4.

[32] P.N. Kaloni and J.X. Lou, "Nonlinear convection of a viscoelastic fluid with inclined temperature gradient". *Contin. Mech.Thermodyn*. 17, 17–27, 2005. DOI: 10.1007/s00161-004-0184-2.

[33] A. Matta, P. A. L. Narayana and A. A. Hill, "Nonlinear thermal instability in a horizontal porous layer with an internal heat source and mass flow," *Acta Mech.*, vol. 227, pp. 1743-1751, 2016. DOI: 10.1007/s00707-016-1591-8.

[34] A. Matta, "Mono-diffusive Hadley-Prats flow in a horizontal porous layer subject to variable gravity and internal heat generation," *Heat Transf.*, vol. 48(4), pp. 1399-1412, 2019. DOI: 10.1002/htj.21438.

[35] J. K. Platten and J. C. Legros, "*Convection in Liquids*," Springer, New York, 2012.

[36] J. P. Larre, J. K. Platten, and G. Chavepeyer, "Soret effects in ternary systems heated from below," *Int. J. Heat Mass Transf.*, vol. 40(3), pp. 545–555, 1997. DOI: 10.1016/0017-9310(96)00125-1.

[37] D. T. J. Hurle, and E. Jakeman, "Soret-driven thermo-solutal convection," *J. Fluid Mech.*, vol. 47(04), pp. 667–687, 1971. DOI: 10.1017/S0022112071001319.

[38] A. Bahloul, N. Boutana, and P. Vasseur, "Double-diffusive and Soret-induced convection in a shallow horizontal porous layer," *J. Fluid Mech.*, vol. 491, pp. 325–352, 2003. DOI: 10.1017/S0022112003005524.

[39] P. A. L. Narayana, P. V. S. N. Murthy, and G. R. S. Reddy, "Soret-driven thermo-solutal convection induced by inclined thermal and solutal gradients in a shallow horizontal layer of a porous medium," *J. Fluid Mech.*, vol. 612, pp. 1–19, 2008. DOI: 10.1017/S0022112008002619.

[40] K. Roy and P. V. S. N. Murthy, "Soret effect on the double diffusive convection instability due to viscous dissipation in a horizontal porous channel," *Int. J. Heat Mass Transf.*, vol. 91, pp. 700–710, 2015. DOI: 10.1016/j.ijheatmasstransfer.2015.08.002.

[41] N. Deepika, "Linear and nonlinear stability of double-diffusive convection with the Soret effect," *Transp Porous Med.*, vol. 121, pp. 93–108, 2018. DOI: 10.1007/s11242-017-0949-2.

[42] G.S.K Reddy, R Ragoju and S. Shekhar, "Thermohaline convection of a casson fluid in a porous layer: Linear and non-linear stability analyses", *Phys. Fluids.*, 35, 094101, 2023. DOI: 10.1063/5.0163731.

[43] D. Reshmi and P.V.S.N. Murthy, The onset of convective instability of horizontal throughflow in a porous layer with inclined thermal and solutal gradients. *Phys. Fluids.*, 30, 074104, 2018. DOI: 10.1063/1.5040901.

[44] M. K. V. Rafeek, G. J. Reddy, A. Matta and **O. Anwar Bég**, "Computation of internal heat source, viscous dissipation and mass flow effects on mono-diffusive thermo-convective stability in a horizontal porous medium layer," *Spec. Top. Rev. Porous Media.*, vol. 14(1), pp. 17–28, 2023. DOI: 10.1615/SpecialTopicsRevPorousMedia.2022043848.

[45] R. Krishnamurti, "Convection induced by selective absorption of radiation: a laboratory model of conditional instability," *Dyn. Atmos. Ocean.*, vol. 27, pp. 367-382, 1998. DOI: 10.1016/S0377-0265(97)00020-1.

[46] B. Straughan, "*The Energy Method, Stability, and Nonlinear Convection*," 2nd. Edn., Springer, New York, 2004.